



City Research Online

City, University of London Institutional Repository

Citation: Stefanidou, S.P. & Kappos, A. J. (2019). Bridge-specific fragility analysis: when is it really necessary?. *Bulletin of Earthquake Engineering*, 17(4), pp. 2245-2280. doi: 10.1007/s10518-018-00525-9

This is the accepted version of the paper.

This version of the publication may differ from the final published version.

Permanent repository link: <https://openaccess.city.ac.uk/id/eprint/21190/>

Link to published version: <https://doi.org/10.1007/s10518-018-00525-9>

Copyright: City Research Online aims to make research outputs of City, University of London available to a wider audience. Copyright and Moral Rights remain with the author(s) and/or copyright holders. URLs from City Research Online may be freely distributed and linked to.

Reuse: Copies of full items can be used for personal research or study, educational, or not-for-profit purposes without prior permission or charge. Provided that the authors, title and full bibliographic details are credited, a hyperlink and/or URL is given for the original metadata page and the content is not changed in any way.

City Research Online:

<http://openaccess.city.ac.uk/>

publications@city.ac.uk

Bridge-specific Fragility Analysis: When is it really necessary?

Sotiria P. Stefanidou¹ and Andreas J. Kappos^{1,2}

¹ Department of Civil Engineering, Aristotle University
Thessaloniki, 54124, Greece
e-mail: ssotiria@civil.auth.gr

² Department of Civil Engineering, City, University of London
London EC1V OHB, UK
e-mail: Andreas.Kappos.1@city.ac.uk

Keywords: Bridges, Assessment, Bridge-Specific Fragility Curves, Limit State Thresholds, Road network.

Abstract. In seismic assessment of bridges the research focus has recently shifted on the derivation of bridge-specific fragility curves that account for the effect of different geometry, structural system, component and soil properties, on the seismic behaviour. In this context, a new, component-based methodology for the derivation of bridge-specific fragility curves has been recently proposed by the authors, with a view to overcoming the inherent difficulties in assessing all bridges of a road network and the drawbacks of existing methodologies, which use the same group of fragility curves for bridges within the same typological class. The main objective of this paper is to critically assess the necessity of bridge-specific fragility analysis, starting from the effect of structure-specific parameters on component capacity (limit state thresholds), seismic demand, and fragility curves. The aforementioned methodology is used to derive fragility curves for all bridges within an actual road network, with a view to investigating the consistency of adopting generic fragility curves for bridges that fall within the same class and quantifying the degree of over- or under- estimation of the probability of damage when generic bridge classes are considered. Moreover, fragility curves for all representative bridges of the analysed concrete bridge classes are presented to illustrate the differentiation in bridge fragility for varying structural systems, bridge geometry, total bridge length and maximum pier height. Based on the above, the relevance of bridge-specific fragility analysis is assessed, and pertinent conclusions are drawn.

1 INTRODUCTION

Reliability of road systems and their components, exposed to multiple natural hazards is at the front line of engineering research during the last three decades, as possible damage to critical components is strongly related to important direct and indirect economic losses. Bridges are considered to be the most critical component of urban and interurban transport systems, ensuring i.a. access to cities affected by a strong earthquake. In this context, numerous methods have been developed for the assessment of seismic vulnerability of bridges, mainly in the form of fragility curves.

Bridge fragility curves are essential for the estimation of the road or railway system's resilience, recovery planning, as well as pre- and post-earthquake retrofit prioritization. Both analytical and empirical fragility curves were proposed by various research groups, the latter being less frequent (e.g. Basoz & Kiremidjian, 1999), since earthquake damage data for bridges is sparse. Analytical methodologies available in the literature can be classified based on whether they consider multiple components (Mander & Basöz (1999), Nielson & DesRoches (2007a), Moschonas et al. (2008), Zhang et al. (2008), Tsionis & Fardis (2012)) or only the most critical one (piers) in fragility analysis (Banerjee & Shinozuka, 2007). Classification can also be based on the procedure for estimation of component or system capacity (limit state thresholds) and seismic demand (analysis method used), the uncertainty treatment and the probabilistic model used (Table 1). Specifically, regarding component capacity, either local (Avşar et al. (2011), Tsionis & Fardis (2012), Choi et al. (2004)) or global (Shinozuka et al. (2000), Cardone (2013)) demand parameters are used, while quantification of damage, namely the limit state thresholds, is commonly based on experimental results (Dutta & Mander (1998), Berry & Eberhard (2003), HAZUS (2015)). Regarding the estimation of seismic demand, different analysis methods have been put forward, namely inelastic static (pushover) analysis (e.g. (Cardone et al. (2007), Moschonas et al. (2008)), elastic response spectrum method (e.g. Mander & Basöz (1999), HAZUS (2015)) and nonlinear response-history analysis (Mackie & Stojadinović (2007), DesRoches et al. (2012)). The maximum likelihood method (Shinozuka et al. 2000) and the probabilistic seismic demand model (Nielson & Desroches 2007b) have been used for the derivation of fragility curves. The way capacity and demand estimation is made in the frame of analytical methodologies for the derivation of fragility curves is summarised in Table 1.

Bridge fragility curves are used in the assessment of seismic performance and losses in bridge stocks providing valuable data for retrofit prioritisation, also in the frame of transportation network recovery planning, strongly related to government investment and decision-making. Therefore, the need for consistent and reliable fragility curves emerges. In a practical context, these curves should be representative of a fairly small number of bridge classes. The most common approach for deriving 'generic' fragility curves is to classify bridges into different typological classes based on key structural and geometric characteristics like structural system, number of spans, number of columns (single or multicolumn bents), skewness, deck type, pier type and the pier-to-deck connection (Avşar et al. (2011), Moschonas et al. (2008), Mander & Basöz (1999), Tsionis & Fardis (2012), DesRoches et al. (2012)) and derive fragility curves for the generic bridge (representative of each class), to be used for the assessment of the bridge stock, under the assumption that the seismic performance of bridges

within the same class is similar. The fragility curves proposed so far are based on analysis of deterministically defined bridge models, accounting for varying geometric and material properties within the probabilistic framework of fragility analysis. Furthermore, parametric vulnerability curves are proposed in the literature (Elnashai et al. 2004) introducing generic fragility functions based on analysis of bridges having different geometries and overstrength ratios. The parametric approach is rather appealing, albeit oversimplified, since neither the effect of different component properties on seismic demand and capacity, nor the effect of different structural configuration on system fragility are captured.

Table 1: Capacity and demand estimation in analytical methodologies for the derivation of fragility curves

Research Group	Capacity		Seismic Demand		
	Engineering Demand Parameter	Limit State thresholds	Structural model	Seismic Input	Analysis Method
1. Avşar <i>et al.</i> (2011)	Piers: φ Beams: φ, V_u Bearings: δ [3 LS]	Piers: Priestley <i>et al.</i> , (1996), Erduran & Yakut, (2004) Bearings: FHWA, (2006)	3D DM	25 accel. (unscaled)	NRHA
2. Banerjee & Shinozuka (2007)	Piers: μ_θ [5 LS]	Dutta, (1999)	3D DM	3×20 accel.	NRHA & CSM
3a. Cardone, Perrone & Dolce (2007), Cardone, Perrone, & Sofia, 2011) Cardone (2013)	Piers: δ Bearings: δ Abutments: δ [3 LS]	Piers: δ_y & δ_u Bearings: γ (%) Konstantinidis <i>et al.</i> (2008) Abutments: δ_{gap} & δ_u	MDOF→SD OF, Adaptive Pushover	Spectrum	CSM (adaptive)
3b. Cardone, Perrone, & Sofia, 2011)	Piers: μ_φ, V Bearings: δ, μ_δ Abutments: F [5 LS]	Piers: $\delta_y, 50\% \mu_\delta, \delta_u$ Bearings: μ_δ Abutments: Active & Passive resistance	MDOF→SD OF, Adaptive Pushover	Spectrum	CSM (adaptive)
4. Choi <i>et al.</i> (2004)	Piers: μ_φ Bearings: δ [5 LS]	Piers: Dutta, (1999) Bearings: Experiments	3D DM	100 synthetic accel.	NRHA
5. Crowley <i>et al.</i> (2011), Tsionis & Fardis (2012)	Piers: θ Bearings: δ [2 LS]	Piers: θ_y & θ_u Biskinis & Fardis, (2010a, b) Bearings: Bousias <i>et al.</i> 2007	SDOF(Long), Beam with springs (Trans)	EC8 elastic spectrum	Equivalent Static
6. De Felice & Giannini (2010)	Piers: θ [2 LS]	θ_y & θ_u	Metamodels	2×4 accel.	NRHA - RSM
7. Dukes (2013)	Piers: μ_φ Bearings: δ Abutments: δ [4 LS]	Piers: Dutta, (1999) Bearings - Abutments: Caltrans (2010)	Metamodels	3×40 accel.	NRHA - RSM
8. Elnashai <i>et al.</i> (2004)	Piers: δ	δ_y & δ_u (Pushover Curve)	3D DM	7 accel. (scaled)	NRHA
9. Ghosh <i>et al.</i> (2013)	Piers: μ_φ Bearings: δ Abutments: δ [4 LS]	Nielson & DesRoches (2007b)	Metamodels	24 accel. (Wen & Wu)	NRHA - RSM

10. Hwang <i>et al.</i> , (2001)	Piers: <i>C/D factors</i> or μ_δ [5 LS]	Piers: δ_y & δ_u	3D DM	100 acc. synthetic	NRHA
11. Karim & Yamazaki (2001,2003)	$DI=(\mu_\delta+\beta\mu_h)/\mu_u$ (Park-Ang) [5 LS]	$DI=0.00\sim 1.00$	SDOF	250 accel.	Nonlinear Static/NRH A
12. Mackie & Stojadinović (2004)	Drift (%)	Berry & Eberhard (2003)	3D DM	80 accel.	NRHA
13. Mander & Basöz (1999)	Piers: δ/h (%) Bearings: δ [5 LS]	Dutta, (1999)	SDOF	Elastic spectrum	CSM
14. Moschonas <i>et al.</i> (2008)	Bridge: δ [5 LS] [5 LS]	Piers: δ_y & δ_u (Pushover curve) Bearings: δ (γ %)	3D DM	Elastic spectrum	CSM
15. Nielson & DesRoches (2007a, b)	Piers: μ_ϕ Bearings: δ Abutments: δ [4 LS]	Piers: HAZUS (1997), FHWA (2006) Bearings, Abutments : Choi (2004)	3D DM	48 accel. (3 bins)	NRHA
16. Ramanathan, (2012)	Piers: μ_ϕ Bearings: δ Abutments: δ [4 LS]	Piers: Berry & Eberhard (2003), Bearings, Abutments : Caltrans (2010)	3D DM	320 accel. (4 bins)	NRHA
17. Shinozuka <i>et al.</i> (2000)	Piers: μ_δ [3 LS]	$1.0 \leq \mu_\delta \leq 2.0$	3D DM	80 accel.	NRHA
18. Tavares <i>et al.</i> , (2012)	Piers: μ_ϕ Bearings: δ Abutments: δ [4 LS]	HAZUS (1997)	3D DM	Synthetic Accel.	NRHA
19. Yi <i>et al.</i> (2007)	Piers: μ_ϕ Bearings: δ	Choi (2004)	2D Model	60 accel.	NRHA
20. Zhong <i>et al.</i> (2012)	Piers: Drift (%)	Probabilistic model (closed form relationship)	3D DM	Elastic spectrum	CSM

* **3D DM**: 3D Detailed Model, **NRHA**: Nonlinear Response History Analysis **CSM**: Capacity Spectrum Method

It is clear that the accuracy and consistency of the assumption that fragility curves of a generic bridge can be used for all bridges within the same class depend on the scope and size of the classification scheme adopted. Moreover, it should be noted that component demand and capacity vary and are related to component-specific properties, while bridge fragility was found to be highly dependent on structure-specific parameters, like deck and pier geometry (Avşar et al. (2011), Tavares et al. (2012), Elnashai et al. (2004)), structural system, which is related to the topography and the construction method selected (Zhang et al., 2008), material and geometric properties of components, as well as parameters related to the foundation soil and the earthquake ground motion selection. The use of modification factors to account for the effect of skewness and site conditions has been proposed (Mander & Basöz, 1999), an appealing but rather oversimplified approach, as discussed in Dukes (2013). As an alternative, the concept of bridge-specific fragility analysis has been put forward (Dukes (2013), Stefanidou & Kappos (2015, 2017)), duly accounting for the effect of component-specific properties on bridge fragility. However, the methodology proposed by Dukes (2013) focuses

on the correlation of component demand and structure-specific parameters, providing demand models as a function of multiple design parameters in the frame of the ‘metamodeling’ concept, not accounting for their effect on component capacity and limit state thresholds. On the other hand, Stefanidou & Kappos (2017) proposed a holistic methodology for the estimation of bridge-specific fragility curves providing empirical relationships for the estimation of component-specific limit state thresholds, uncertainty treatment and demand estimation, the amount of effort depending on the application scale (single bridge or bridge stocks).

The main objective of this paper is to put into context the relevance of bridge-specific fragility analysis when an entire stock is addressed. Initially the effect of structure-specific parameters on component capacity (limit state thresholds), seismic demand, and fragility curves is established. The effect of pier properties on limit state thresholds is evaluated for different concrete pier types, considering both local and global demand parameters. The recently proposed (by the authors) methodology (Stefanidou & Kappos, 2017) is then applied (using ad-hoc developed software) for the estimation of fragility curves for all bridges of an actual road network, using the simplified approach, while uncertainty in demand estimation is quantified based on the detailed approach entailing advanced analysis. Bridge-specific fragility curves for all representative bridges of the different concrete bridge classes are presented, to highlight the effect of structural system (different pier, deck and pier-to-deck connection types) on bridge fragility. The effect of bridge geometry, namely total bridge length and maximum pier height, on bridge fragility is evaluated through analysis of all bridges (and bridge classes) of the road network under consideration. Subsequently, the consistency of adopting generic fragility curves for bridges that fall within the same category is assessed, by quantifying the degree of over- or under- estimation of the probability of damage when generic bridge classes are used. The conclusions of this study refer to the concrete bridge stock studied (described in detail in §4.2.1), which is typical of Southern Europe motorways. Nevertheless, the proposed methodology for bridge-specific fragility analysis has a broad application range and could be used for the seismic assessment of any other bridge stock.

2 METHODOLOGY FOR DERIVING BRIDGE-SPECIFIC FRAGILITY CURVES

The methodology proposed by the authors for the derivation of bridge-specific fragility curves and the successive steps for its implementation are described in detail elsewhere (Stefanidou & Kappos, 2017). It is noted that a key aspect of the methodology is that it does not depend on the structural system and bridge properties, minimising the need for classification to typological classes. The methodology, outlined in the flowchart of Fig.1, is component-based and entails closed-form relationships for defining component-specific limit state thresholds (component database) and two alternatives for the calculation of seismic demand based on analysis of a detailed or simplified bridge model, depending on whether a single bridge or a bridge stock is addressed. Obviously, the question of whether bridge-specific analysis is really necessary arises when entire stocks are analysed, hence the basic principles for the estimation of component capacity (database development) and seismic demand briefly described in the remainder of this section refer to this case; more details of both versions of the methodology are found in Stefanidou & Kappos (2017).

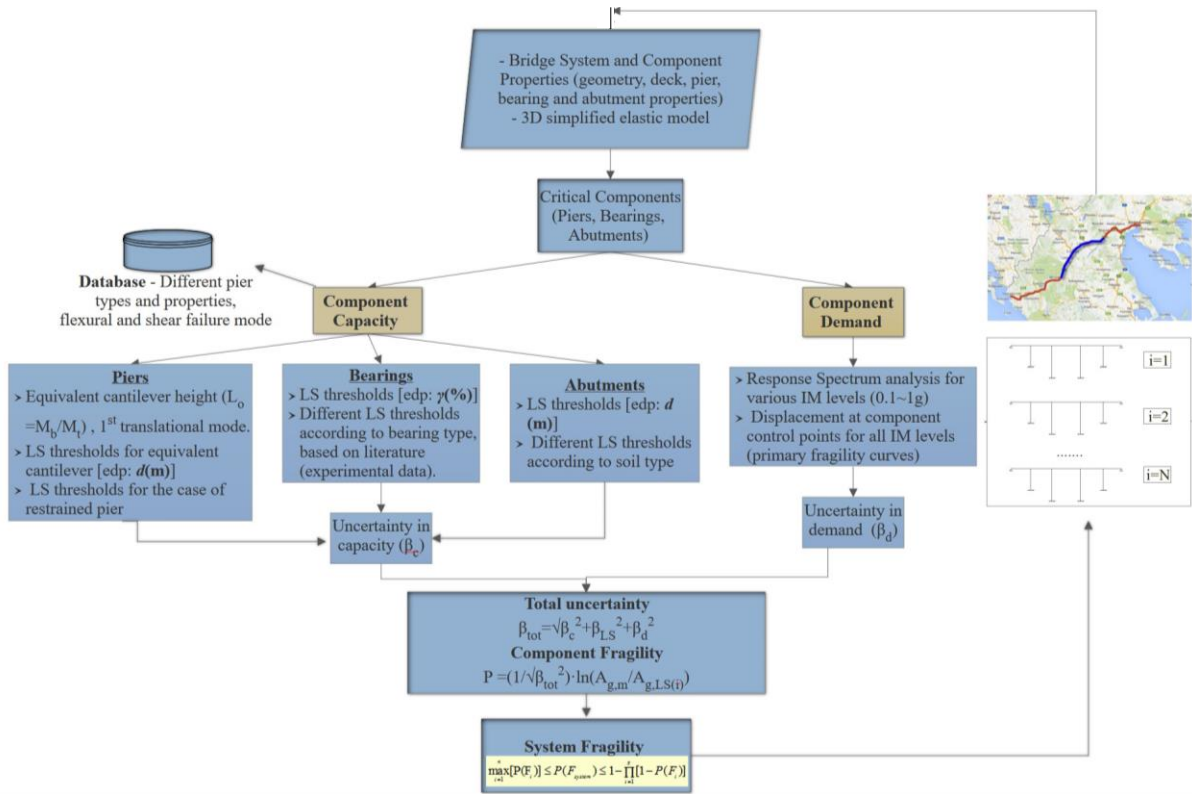


Fig. 1 – Flowchart of the component-based methodology for the derivation of bridge-specific fragility curves applied to a population of bridges

2.1 Bridge capacity

As depicted in Table 1, different global or local demand parameters (EDP) are utilised in existing methodologies for the quantification of component damage, while threshold values are in most cases based on experimental results. Whenever analytical estimation of limit state thresholds is proposed, component-specific analysis is required, rendering the methodology case-dependent and increasing the computational cost.

In the frame of the proposed methodology, bridge piers, abutments and bearings are considered as critical components affecting the system’s seismic performance, and limit state thresholds for four limit states are explicitly defined based on inelastic analysis results and/or experimental data, depending on the component examined. The milestone of the proposed methodology as far as capacity estimation is concerned, is that the user can define component limit state thresholds considering all different component properties that may affect inelastic behaviour, without performing inelastic analysis for each component. To this end, a database of different components has been developed, based on multiple parametric inelastic analyses (considering different possible failure modes) to derive limit state thresholds. Based on regression analysis of the results, closed-form relationships were derived for limit state thresholds, based on various parameters affecting capacity of different component types. Hence, irrespectively of the procedure followed for fragility estimation, a reliable methodology for limit state threshold (capacity) estimation is provided.

Regarding the component which is usually the most critical for the seismic response, namely bridge piers, the procedure followed for the development of the database is presented in Fig. 2. The steps for the compilation of the database are:

- (a) Consideration of different concrete pier types, encompassing practically all common types found in a European bridge stock. Cylindrical, hollow cylindrical, rectangular, hollow rectangular and wall-type piers are considered herein. It should be mentioned that hollow rectangular and wall piers are commonly designed to remain elastic (especially in bridges with pier-to-deck connection through bearings), nevertheless their inelastic behaviour was studied to quantify all limit state thresholds.

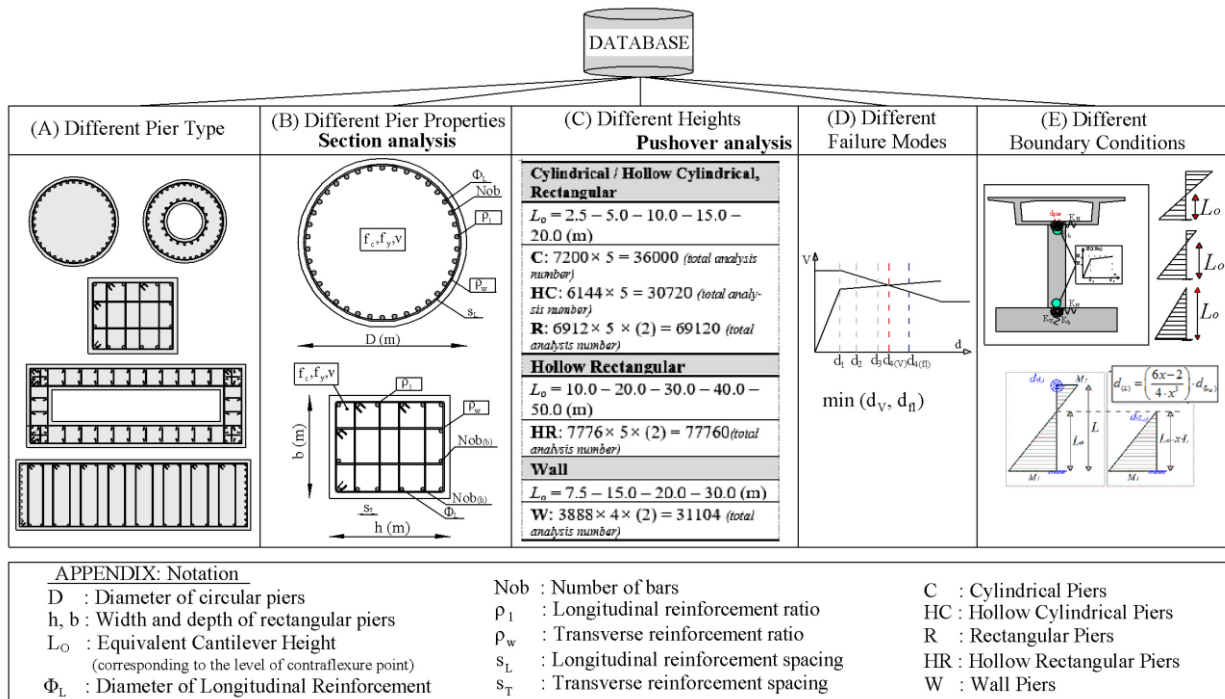


Fig. 2 – Procedure for development of database for bridge piers (details provided in Stefanidou & Kappos (2017))

- (b) Consideration of pier cross section parameters, namely dimensions, longitudinal and transverse reinforcement ratio, normalised axial force, and material properties. Section analyses are performed for all relevant combinations of parameters considering confined and unconfined concrete material laws. Specifically, for confined concrete the Mander et al. (1988) model is used for cylindrical sections, the Priestley & Ranzo (2000) model for hollow cylindrical sections, and the Kappos (1991) model for rectangular, hollow rectangular, and wall sections. Parametrically defined input cross section files are set up and multiple section analyses are performed using the software AnySection (Papanikolaou, 2012). Pier damage is initially defined at cross section level, using local demand parameters (section curvature, ϕ), related to experimentally estimated damage (e.g. crack widths) via section analysis, therefore limit state thresholds in curvature (local) terms (Table 2) are defined within this step.
- (c) Consideration of a sufficiently broad range of heights for each pier section type and parametric setup of an inelastic cantilever model in order to perform pushover analysis and define limit state thresholds in terms of a global demand parameter (displacement of control point). Plastic hinge formation is considered at the cantilever base (lumped plasticity model), whereas the M- ϕ curve, calculated at step (b), is used as input.

Inelastic static analysis is performed for all sections considered (strong and weak section direction analysed separately) paired with all different pier heights, using a Matlab-based code developed for the setup of input files, and Opensees (McKeena & Fenves, 2015) for inelastic static analysis. Limit state thresholds in *global* terms (displacement of control point for limit states 1 to 4) are correlated to *local* ones (curvature for limit states 1 to 4), using the results of inelastic pushover analysis, additionally considering P-delta effects.

- (d) Check for shear failure, calculating the displacement when shear strength V_u is developed (d_v), considering reduced concrete contribution in the inelastic range (Fig. 2(D)); d_v is compared with the displacement at flexural failure (d_{fl}) and the minimum value is considered as threshold value for the limit state (Table 2). V_u is calculated according to Priestley et al. (1996), i.e.

$$V_u = V_c + V_w + V_p \quad (1)$$

where, V_c is the shear resistance of concrete mechanisms, V_s the contribution of the transverse reinforcement and V_p is the shear carried by the axial load.

Based on inelastic static analysis results, limit state thresholds are defined in displacement terms for all different pier types, section properties and heights considered (d_1 to d_4 for all cases described within steps a-d), and regression analysis is performed to derive closed-form relationships for each pier type and limit state.

- (e) Since all previous steps are based on the analysis of an inelastic cantilever model, the effect of different boundary conditions on limit state thresholds should also be considered. In general, bridge piers are restrained at the top (depending on the type of pier-to-deck connection and the rotational stiffness of the deck) and at the bottom, the latter depending on the foundation type and ground properties. The tip displacement of the equivalent cantilever (height equal to the height of contraflexure point calculated for each case as pier top to bottom moment ratio, from elastic analysis) is related to the displacement of the restrained pier, as shown in Fig. 2(E).

For the quantification of abutment and bearing damage, threshold limit state values are defined in terms of displacement of the component control point, based on experimental data and other information from the literature, as described in Stefanidou & Kappos (2017) and summarised in Table 2.

Threshold displacement values for seat-type abutments are related to the curvature ductility (for LS1) and backwall height (for LS2 to LS4); integral abutments are not considered herein. Since curvature ductility is related to backwall inelastic performance and properties ($M-\phi$ curve), correlation to gap size (of the abutment joint) is also made, to allow easy definition of the threshold limit state value for LS1, avoiding inelastic analysis of the backwall in each application. To this end, parametric analyses of abutment (component) models were performed, considering varying backwall heights and section properties, as well as different backfill soil properties. Based on these analyses, the displacement corresponding to $\mu_\phi=1.5$ was found to be approximately equal to $1.1d_{gap}$ (values ranged from 1.04 to $1.2d_{gap}$) (Table 2).

Table 2. Limit state thresholds for critical structural components

Limit State	R/C Piers / EDP: d (m)		Abutments	Bearings
	<i>Local</i>	<i>Global</i>	EDP: d (m)	EDP: γ (%)
LS 1 – Minor/Slight damage	$\varphi_1: \varphi_y$	$d_1: \min \begin{Bmatrix} d(\varphi_1) \\ d(V_1) \end{Bmatrix}$	$d_1 = 1.1 \cdot d_{gap}$ ($\mu_{\varphi,bw} = 1.5$)	20 ($d_1 = 0.02 \cdot h_{br}$)
LS 2 – Moderate damage	$\varphi_2: \min (\varphi: \varepsilon_c > 0.004 ,$ $\varphi: \varepsilon_s \geq 0.015)$	$d_2: \min \begin{Bmatrix} d(\varphi_2) \\ d(V_2) \end{Bmatrix}$	$d_2 = 0.01 \cdot h_{bw}$	100 ($d_2 = 0.1 \cdot h_{br}$)
LS 3 – Major/Extensive damage	$\varepsilon_c \leq 0.004 +$ $\varphi_3: \min (\varphi:$ $1.4 \cdot \rho_w \cdot \frac{f_{yw}}{f_{cc}}$ $\varphi: \varepsilon_s \geq 0.06)$	$d_3: \min \begin{Bmatrix} d(\varphi_3) \\ d(V_3) \end{Bmatrix}$	$d_3 = 0.035 \cdot h_{bw}$	200 ($d_3 = 0.2 \cdot h_{br}$)
LS 4 – Failure/Collapse	$\varphi_4: \min (\varphi:$ $M < 0.90 \cdot M_{max} , \varphi:$ $\varepsilon_s \geq 0.075)$	$d_4: \min \begin{Bmatrix} d(\varphi_4) \\ d(V_4) \end{Bmatrix}$	$d_4 = 0.1 \cdot h_{bw}$	300 ($d_4 = 0.3 \cdot h_{br}$)

*bw: backwall

Threshold displacement values for elastomeric bearings are related to shear strain, estimated from experimental data (Table 2). For the case of lead rubber bearings, limit state thresholds are differentiated mainly regarding LS1 (Stefanidou & Kappos, 2017), associated with the shear strain corresponding to lead core yielding. It should be noted that for both elastomeric and lead rubber bearings, attainment of the buckling load (P_{cr}) is also checked, while pot bearings, allowing sliding in one or both directions are not considered as critical components. At this stage of development the database does not include ‘old-type’ steel bearings found in pre-1980 concrete bridges or special isolation bearings other than lead rubber ones.

Based on the above, a database of critical components was developed, providing component-specific limit state thresholds (as described in §3), for calculating component capacity and the associated uncertainty β_C . A website is currently being developed, providing all information regarding the database compilation, namely software developed for multiple parametric inelastic static component analysis and analytical limit state threshold definition (Stefanidou, 2017), experimental data collected for quantitative damage definition, etc. The site will eventually provide an online platform, allowing component-specific limit state threshold quantification (based on the closed-form relationships provided in §3) in the frame of fragility analysis, avoiding both time-consuming inelastic analyses and the need for approximate definition of capacity regardless of the properties of the component, which affect the reliability of fragility analysis. Moreover, it will be interactive allowing input from users/contributors with a view to enriching the database and receiving feedback.

2.2 Seismic demand

In the frame of the ‘general’ methodology, the calculation of seismic demand at the component control point is differentiated depending on the application scale (single bridge or bridge stock). Bridge-specific fragility curves for a single bridge entail nonlinear response

history analysis of a detailed inelastic model, using an enhanced IDA procedure described in Stefanidou & Kappos (2017) (IDA combined with multiple stripe analysis), in order to estimate seismic demand at component control points for different levels of earthquake intensity. Uncertainty in seismic demand (logarithmic standard deviation β_D) is calculated for each critical component (with random properties), also accounting for record-to-record variability. Since the application of the methodology to bridge stocks for the derivation of bridge-specific fragility curves is computationally demanding, the procedure proposed for bridge stock analysis (described in Stefanidou & Kappos (2017)) is applied, and response spectrum analysis of a simplified elastic model using the Eurocode 8 spectrum for varying levels of earthquake intensity is invoked (scaling PGA, typically from 0.1g to 1g) to estimate seismic demand at component control points; the evolution of damage with earthquake intensity is plotted for each component considered (mean value). Bridge-specific fragility curves are plotted assuming lognormal distribution, while uncertainty in seismic demand (β_D), calculated for generic bridges representative of a specific bridge class according to the classification system proposed by Moschonas et al. (2008), is used as dispersion value. It is clear that in practical fragility analysis it is not feasible (nor desirable) to estimate uncertainty through Monte Carlo analysis (even with reduced sampling) of each individual bridge; β values should inevitably come from a classification-based approach.

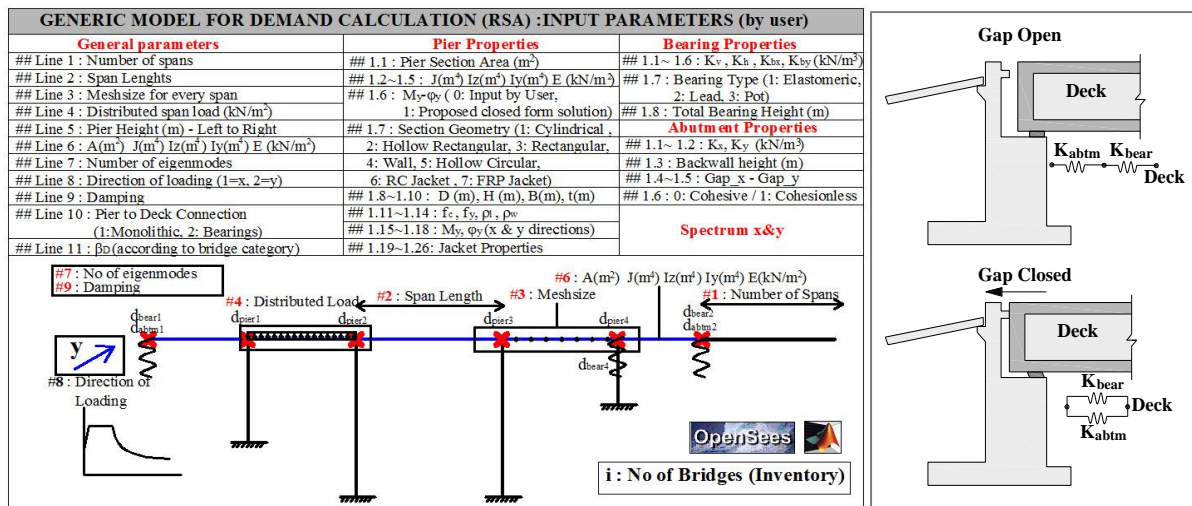


Fig. 3 – Software for bridge-specific fragility curves (input data – cases of open/closed gap)

For bridge stock analysis, a Matlab-based software is developed for the derivation of bridge-specific fragility curves. The software is based on a generic (parametrically defined), simplified 3D bridge model created using the OpenSees platform (McKeena & Fenves, 2015) according to bridge-specific, user-defined properties. The methodology described in Stefanidou & Kappos (2017) for single bridge analysis is embedded in the software; component-specific limit state thresholds are calculated based on user-defined properties and multiple response spectrum analyses for varying levels of earthquake intensity are performed for demand estimation. Different boundary conditions at abutments are considered for the case of open and closed gap, while fragility curves are automatically derived and plotted for each component, separately for the longitudinal and transverse directions. Bridge-specific fragility curves for the entire bridge are calculated and plotted, under the assumption of series

connection between components (lower bound), except for LS4, where piers or abutments are considered as critical components. Detailed description of the software developed can be found elsewhere (Stefanidou, 2017).

3 SEISMIC CAPACITY ASSESSMENT (DATABASE FOR LIMIT STATE THRESHOLDS)

The first step to gain insight into the relevance of bridge-specific fragility analysis, is to evaluate the effect of varying properties on component capacity, which is related to the limit state thresholds, or, in other words, to component damage for the limit states considered. To this end, different pier types and properties are considered, in the frame of the methodology proposed by Stefanidou & Kappos (2017), with a view to developing a database encompassing practically all common concrete pier types found in a bridge stock. The effect of varying pier properties on limit state thresholds is evaluated herein for different pier types and the results, considering both local and global demand parameters, are discussed.

A broad range of different section properties, namely dimensions, longitudinal and transverse reinforcement ratio, normalised axial force and material properties are considered, and section analysis is performed as described in §2.1(b). Damage is initially quantified using material strain values, namely ε_c and ε_s corresponding to experimentally observed crack widths, and moment corresponding to loss of bearing capacity for limit state 4 (post-peak $M=0.9 \cdot M_{\max}$). Based on cross section analysis, moment-curvature curves are calculated (and bilinearised) and curvature values corresponding to the aforementioned material strains are defined. Hence, damage is initially defined in curvature terms (*local* EDPs $\varphi_1, \varphi_2, \varphi_3, \varphi_4$), and M - φ curves as well as effective stiffnesses EI_{eff} (M_y/φ_y), needed for pushover analysis, are defined.

Section analysis results for all possible parameter combinations (nearly 8000 section analyses for each pier type considering weak and strong section axes separately), are obtained for each pier type and regression analysis is performed. As an example, closed-form relationships for φ_y, φ_u and M_y, M_u are presented in Table 3 for cylindrical piers; relevant relationships are available for all different pier types, however a detailed presentation is beyond the scope of this paper (it will be made available on the aforementioned website).

Table 3. Closed-form relationships for the estimation of moment vs curvature for cylindrical piers

	β_0	β_1	β_2	β_3	β_4
$\varphi/D = \exp[\beta_0 + \beta_1 \cdot \ln(f_c / f_y) + \beta_2 \cdot \ln(v) + \beta_3 \cdot \ln \rho_l + \beta_4 \cdot \ln \rho_w]$					
$M/2 \cdot \pi \cdot R^3 \cdot f_{cd} = \exp[\beta_0 + \beta_1 \cdot \ln(f_c / f_y) + \beta_2 \cdot \ln(v) + \beta_3 \cdot \ln \rho_l + \beta_4 \cdot \ln \rho_w]$					
φ_y	-5.716	-0.734	-0.017	+0.309	+0.089
φ_u	-2.331	-0.602	-0.582	-0.049	+0.602
M_y	-0.369	-0.633	+0.225	+0.551	+0.053
M_u	-0.269	-0.645	+0.217	+0.559	+0.054

The effect of varying cross section parameters on local demand parameters (φ or μ_φ values) is depicted in Figures 4 and 5 for cylindrical piers and Fig. 6 for different pier types,

highlighting the over- or under-estimation of threshold values in case that a uniform value, irrespective of section properties, is considered.

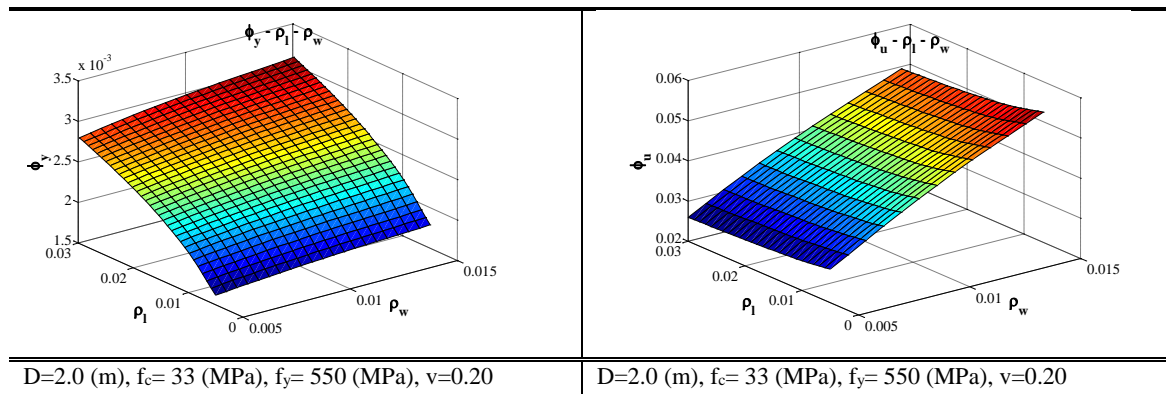


Fig. 4 – Effect of longitudinal and transverse reinforcement ratio on yield (left) and ultimate (right) curvature of cylindrical sections

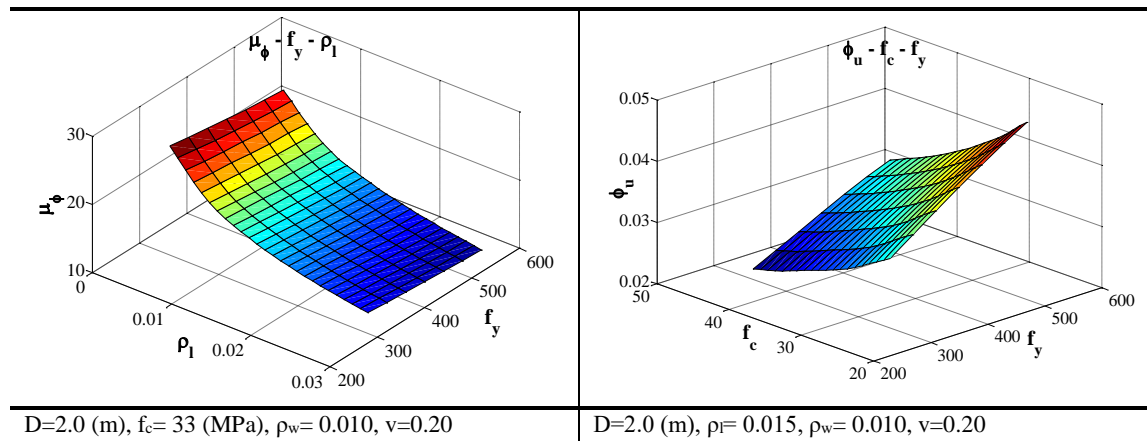


Fig. 5 – Effect of steel strength and longitudinal reinforcement ratio on curvature ductility (left) and steel and concrete strength on ultimate curvature (right) of cylindrical sections

As shown in Fig. 4, yield curvature increases for increasing longitudinal reinforcement ratio (ρ_l), while the effect of transverse reinforcement ratio (ρ_w) is negligible. On the contrary, ultimate curvature is highly affected (increased for increasing transverse reinforcement), due to the relevant increase in ultimate concrete strain (ϵ_{cu}) caused by confinement. The effect of concrete and steel strength on ultimate curvature is depicted in Fig. 5(right). Based on the above, curvature ductility decreases for increasing longitudinal reinforcement ratio ($\mu_\phi = \phi_u / \phi_y$ – Fig. 5(left)), while this effect is more pronounced for $\rho_l > 0.01$.

It is evident from Fig. 6 that an increase in compressive axial load (v_d) results in decrease of curvature ductility, due to the associated increase in compression zone depth (x_u). Moreover, as shown in Fig. 6, the effect of transverse reinforcement on available curvature ductility is more pronounced for lower values of compressive axial load.

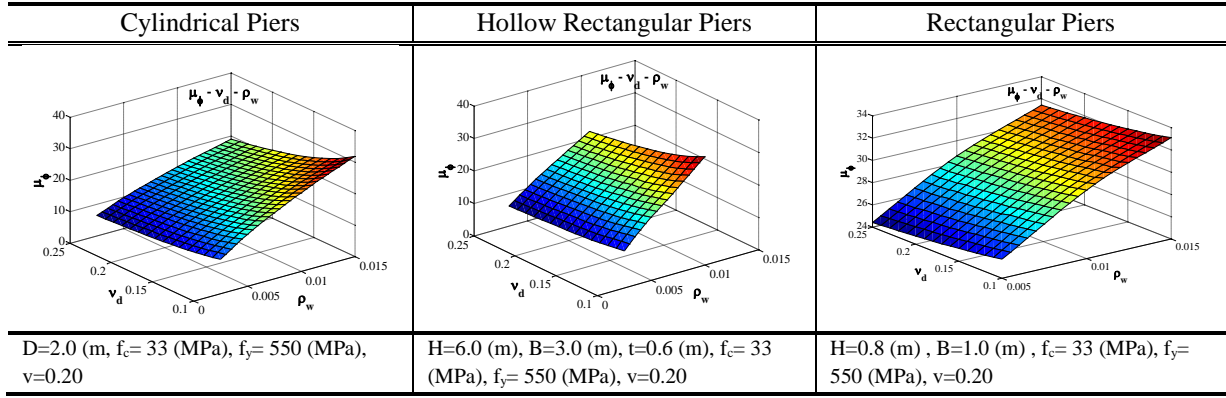


Fig. 6 – Effect of normalised axial force and transverse reinforcement ratio on curvature ductility of cylindrical, hollow cylindrical and rectangular sections

Table 4. Closed-form relationships for limit state thresholds of different pier types

Cylindrical Piers	$\delta/H = \exp[\beta_0 + \beta_1 \cdot \ln(D/H) + \beta_2 \cdot \ln(\nu) + \beta_3 \cdot \ln(f_c/f_y) + \beta_4 \cdot \ln \rho_w + \beta_5 \cdot \ln \rho_l]$
Hollow Cylindrical Piers	$\delta/H = \exp[\beta_0 + \beta_1 \cdot \ln(D/H) + \beta_2 \cdot \ln(D_{in}/D_{out}) + \beta_3 \cdot \ln(\nu) + \beta_4 \cdot \ln(f_c/f_y) + \beta_5 \cdot \ln \rho_w + \beta_6 \cdot \ln \rho_l]$
Hollow Rectangular Piers (Strong Direction)	$\delta/H = \exp[\beta_0 + \beta_1 \cdot \ln(h/H) + \beta_2 \cdot \ln(h/b) + \beta_3 \cdot \ln(h/t) + \beta_4 \cdot \ln(\nu) + \beta_5 \cdot \ln(f_c/f_y) + \beta_6 \cdot \ln \rho_w + \beta_7 \cdot \ln \rho_l]$
Rectangular Piers (Strong Direction)	$\delta/H = \exp[\beta_0 + \beta_1 \cdot \ln(h/H) + \beta_2 \cdot \ln(b/h) + \beta_3 \cdot \ln(\nu) + \beta_4 \cdot \ln(f_c/f_y) + \beta_5 \cdot \ln \rho_w + \beta_6 \cdot \ln \rho_l]$
Wall Piers (Strong Direction)	$\delta/H = \exp[\beta_0 + \beta_1 \cdot \ln(h/H) + \beta_2 \cdot \ln(h/b) + \beta_3 \cdot \ln(\nu) + \beta_4 \cdot \ln(f_c/f_y) + \beta_5 \cdot \ln \rho_w + \beta_6 \cdot \ln \rho_l]$

All different pier sections considered within the database are paired with a sufficiently broad range of pier heights, and pushover analyses are performed (Fig. 2) to correlate local to global demand parameters and quantify damage in terms of displacement of the control point (*global* parameter values d_1 , d_2 , d_3 , and d_4). The possibility of different failure modes (flexure, shear) as well as P-delta effects are accounted for, while the number of analyses varies from 30000 to approximately 78000, depending on pier type and range of heights considered. It should be noted that various equivalent cantilever heights should additionally be considered, to account for different boundary conditions as described in §2.1(e) and Fig. 2(E). From equivalent cantilever analysis, closed-form relationships are derived for each pier type and limit state (d_1 , d_2 , d_3 , d_4), given in Table 4. The pertinent coefficient values (β_i) for all pier types and both strong and weak direction can be found in Annex A; as an illustration, β_i values are provided for cylindrical piers in Table 5.

The effect of varying cross section parameters on global demand parameters (δ or μ_δ) is depicted in Figures 7 and 8; similar remarks apply as in the case of local demand parameters. Threshold values in terms of drift for limit state 4 increase for increasing transverse reinforcement ratio (ρ_w) due to the increase in ultimate curvature, while the effect of longitudinal reinforcement ratio (ρ_l) is negligible. The latter remark is consistent with pertinent experimental results (Lu et al., 2005). On the contrary, regarding limit state 1, the effect of

longitudinal reinforcement ratio (ρ_l) on drift value is more significant, as this affects the yield curvature.

Table 5 – Limit state thresholds for cylindrical piers (in *global* demand terms)

$\delta/H = \exp[\beta_0 + \beta_1 \cdot \ln(D/H) + \beta_2 \cdot \ln(v) + \beta_3 \cdot \ln(f_c/f_y) + \beta_4 \cdot \ln \rho_w + \beta_5 \cdot \ln \rho_l]$							
	β_0	β_1	β_2	β_3	β_4	β_5	R^2
δ_1/H	-6.524	-0.876	-0.018	-0.688	+0.086	+0.292	0.87
δ_2/H	-6.016	-0.674	-0.265	-0.076	+0.030	-0.072	0.88
δ_3/H	-3.872	-0.572	-0.238	-0.470	+0.505	-0.108	0.89
δ_4/H	-3.663	-0.542	-0.381	-0.518	+0.439	+0.001	0.85

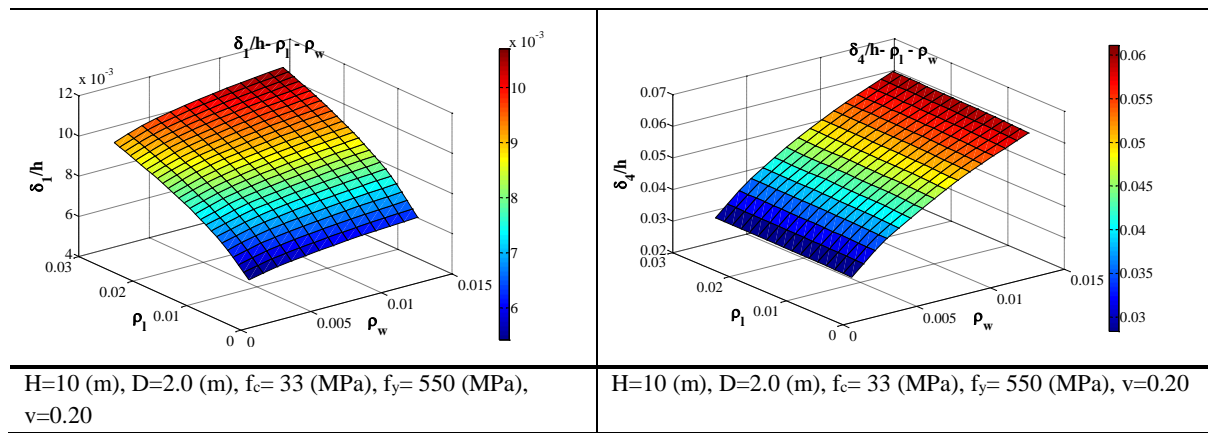


Fig.7 –Effect of longitudinal and transverse reinforcement ratio on δ_1/h (left) and δ_4/h (right) value of cylindrical sections

Displacement ductility increases for increasing transverse reinforcement ratio (ρ_w) and slightly decreases for increasing longitudinal reinforcement ratio (ρ_l) as depicted in Fig. 8 and supported by experimental results (Lee et al., 2014). Moreover, increase in compression axial load and shear span length results in decreased displacement ductility, again consistently with pertinent experimental findings (Lee et al., (2014), Erduran & Yakut, (2004)) and standard mechanics.

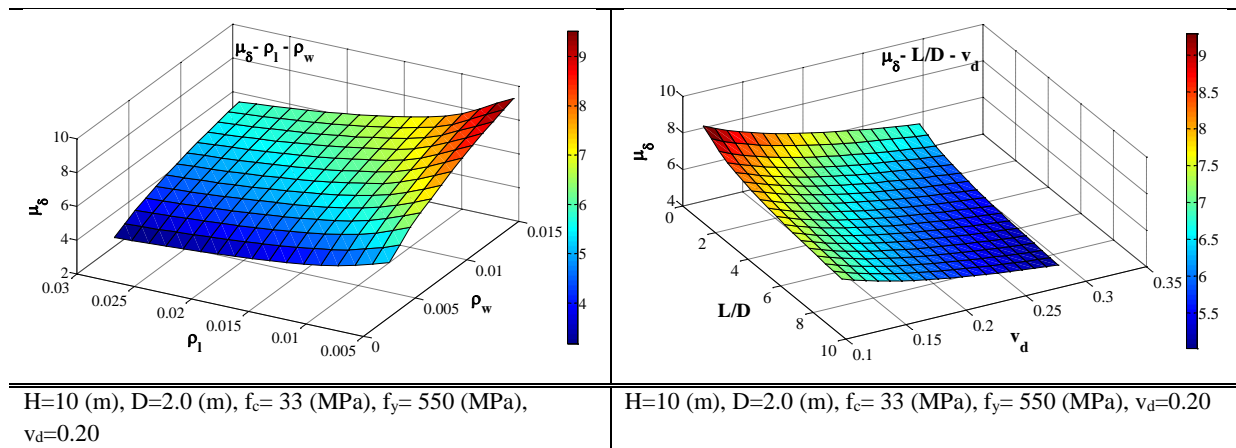


Fig. 8 – Effect of longitudinal and transverse reinforcement ratio (ρ_l and ρ_w), shear span ratio (L/D) and normalised axial load (v_d) on displacement ductility of cylindrical piers (EDP: μ_δ)

4 SEISMIC DEMAND ASSESSMENT (UNCERTAINTY IN SEISMIC DEMAND)

In bridge fragility analysis the seismic demand at component control points (see section 2) has to be defined. The methodology proposed for bridge-specific fragility analysis entails two alternative approaches for demand estimation, related to whether a single bridge or a bridge stock is addressed. Within bridge stock analysis (simplified approach), component demand is calculated based on elastic response spectrum analysis results of the simplified model (described in Fig. 3), while a reliable estimation of uncertainty in seismic demand (β_D) is based on single bridge analysis (detailed approach). To this end a classification-based procedure is used to quantify uncertainty in seismic demand for the representative bridges of the most frequent classes based on nonlinear response history analysis results of the inelastic model and eventually provide β_D values for bridge-specific fragility analysis of bridge stocks using the simplified model and elastic response spectrum analysis. This is the most refined method for β_D quantification, based on analysis results, rather than literature recommendations (many past studies relied on HAZUS, 2015).

The bridge inventory considered herein is part of Egnatia Motorway in Greece, a typical modern motorway in Southern Europe. Bridge-specific fragility curves for all bridges of the road network are provided in a following section (§5) based on the simplified approach, while the variation of dispersion value β_D (uncertainty in demand) within different bridge classes (and critical components) is discussed herein, based on the detailed approach and inelastic dynamic analysis of refined bridge models. Representative bridges of three common classes in the stock are considered and the effect of structural configuration and component-specific properties on uncertainty in demand is evaluated at component and system level.

4.1 Classification of bridge stock

The bridges of the inventory, classified into categories according to an enhanced version of the classification scheme proposed by Moschonas et al. (2009) are summarised in Table 6; the scheme is tailored to the typologies common in medium and high seismicity areas of Europe. A code number ($X_1X_2X_3$) is defined for each bridge according to the pier, deck, and pier-to-deck connection, type. It is noted that, in principle, classification of bridges is not necessary for the application of the methodology proposed for the derivation of bridge-specific fragility curves. However, for reasons of practicality (explicit quantification of uncertainty is time consuming), bridges that fall within the same category are assumed to have the same uncertainty in demand; hence the need for classification.

All different bridge classes of the studied section of Egnatia Motorway are presented in Fig. 9. Prestressed concrete box-girder bridges with hollow rectangular piers monolithically connected to the deck, constructed using the cantilever method, constitute the most frequent typology (25%) due to the site topography (mountainous area). Simply-supported bridges, where the prestressed concrete beam deck is supported on hollow rectangular piers through elastomeric bearings, are the second most frequent class in the stock, while single span overpasses and box-girder bridges with cylindrical single-column or multi-column piers monolithically connected to the deck are also frequently encountered in this stock.

Table 6 – Classification scheme for concrete bridges

X ₁		X ₂		X ₃	
Pier Type		Deck type		Pier-to-deck connection	
Code Number	Description	Code Number	Description	Code Number	Description
1	Single column - Cylindrical section	1	Slab (solid or with voids)	1	Monolithic
2	Single column - Hollow section	2	Box girder	2	Through bearings
3	Multi-column bent	3	Simply-supported precast post-tensioned beams	3	Combination of monolithic and bearing connections
4	Wall-type				
5	V-type				

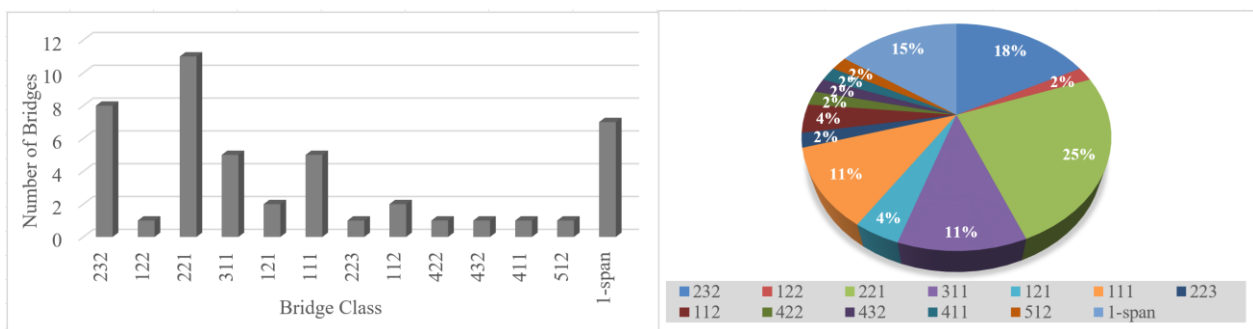


Fig. 9 – Different bridge classes in Egnatia Motorway, Western Macedonia section

4.2 Uncertainty in seismic demand for different bridge classes

The detailed approach (single bridge analysis) was applied to three case-study bridges (assigned to different classes according to the classification system described in §4.1) to quantify uncertainty in seismic demand, also considering uncertainty due to record-to-record variability. The calculation of seismic demand in the case of single bridge assessment is based on the results of nonlinear response history analysis of a detailed inelastic model. Specifically, seismic demand is calculated at the control point of each critical component (piers, bearings and abutments) for different levels of earthquake intensity, using an enhanced IDA procedure (see §2.2). Multiple analyses of statistically different, yet nominally identical, bridge samples are performed and displacements of component control points are recorded and compared to limit state thresholds to calculate the mean a_g for each limit state. The dispersion in seismic demand, i.e. the logarithmic standard deviation (β_D), is also calculated for each component. As noted earlier, the calculation of dispersion is computationally demanding, and in the context of bridge stock analysis, β_D can be assumed to be the same for bridges within the same class.

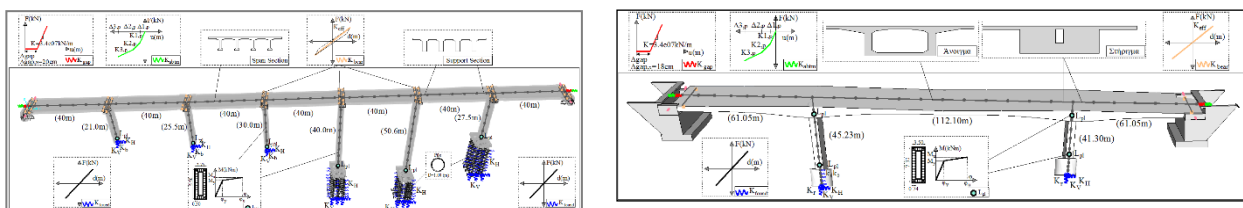


Fig. 10– Case Studies of Egnatia Motorway Bridges (category type 232(left), category type 221(right))

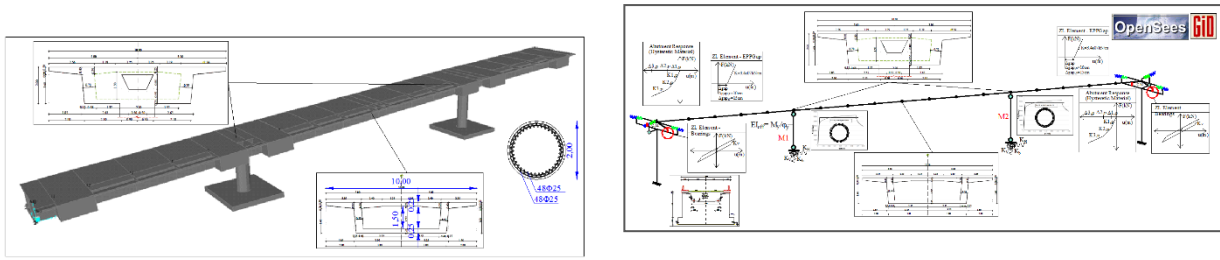
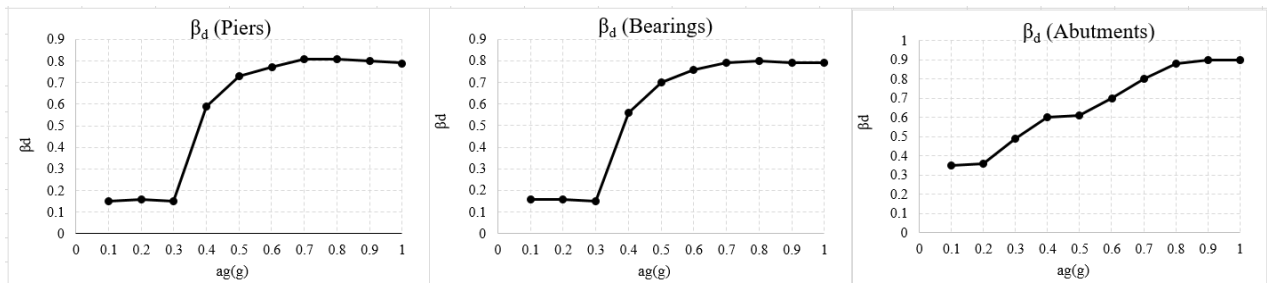


Fig. 11 – Case Study of Egnatia Motorway Bridges (category type 121)

The three different case-study bridges analysed herein, are representative bridges of the classes: simply-supported girder bridge (type 232), prestressed concrete box girder bridge (type 221) and overpass (type 121) (Figures 10, 11). Uncertainty in seismic demand is calculated for different levels of earthquake intensity and all critical components, and the relevant results are presented in Table 7 for a common bridge type (232) and Fig. 12 for bridge type 121 (values given for each component and level of earthquake intensity). It is seen that uncertainty in seismic demand varies, depending on the bridge type, the component considered, and earthquake intensity. In general, uncertainty in demand increases for increased earthquake intensity. It is emphasised that the variation in β_D values is mainly due to record-to-record variability (three earthquake groups and different earthquake motion selection criteria for each group as described in Stefanidou & Kappos, (2017)), while it is also affected by the level of inelasticity in the component studied.

Table 7. Component and system β_D values for typical simply-supported bridge (type 232)

Longitudinal Direction											
Component	β_d (0.1g)	β_d (0.2g)	β_d (0.3g)	β_d (0.4g)	β_d (0.5g)	β_d (0.6g)	β_d (0.7g)	β_d (0.8g)	β_d (0.9g)	β_d (1.0g)	β_d
Piers	0.45	0.44	0.46	0.82	0.81	0.81	0.85	0.89	0.87	0.86	0.73
Bearings	0.37	0.41	0.43	0.84	0.86	0.85	0.84	0.83	0.82	0.81	0.71
Abutments	--	--	0.25	0.28	0.30	0.48	0.55	0.83	0.83	0.82	0.51
Transverse Direction											
Component	β_d (0.1g)	β_d (0.2g)	β_d (0.3g)	β_d (0.4g)	β_d (0.5g)	β_d (0.6g)	β_d (0.7g)	β_d (0.8g)	β_d (0.9g)	β_d (1.0g)	β_d
Piers	0.45	0.44	0.45	0.82	0.80	0.79	0.84	0.82	0.80	0.85	0.71
Bearings	0.44	0.42	0.42	0.84	0.85	0.84	0.79	0.78	0.77	0.77	0.69
Abutments	0.16	0.15	0.18	0.49	0.49	0.49	0.46	0.45	0.44	0.46	0.38



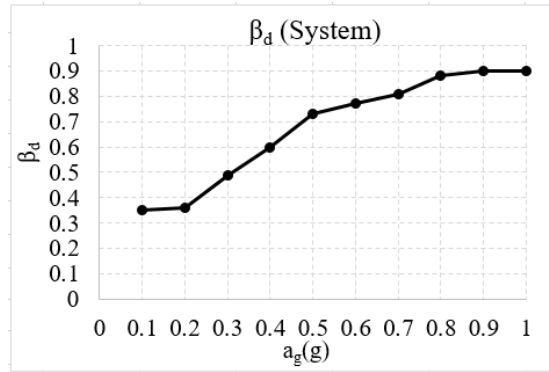


Fig. 12 – Component and system β_D values for typical overpass (type 121)

Uncertainty in seismic demand, i.e. β_D values for all critical components and bridge types considered, are summarised in Table 8 based on bridge-specific fragility analysis of the representative bridge in each class. As shown in Table 8, the β_D value for the system is related to the most critical component (varying with the structural system), while the assumption of a uniform (average) β_D value for the longitudinal and transverse direction in each bridge class appears to be consistent, since differences are mainly up to 15%. Nevertheless, it should be noted that this consistency should be related to the consideration of a uniform β_D value for the system at all levels of earthquake intensity; note that using a single value for all curves is not only simpler but also prevents the not uncommon situation of intersecting fragility curves (due to the different β_D), which lacks physical meaning and leads to inconsistent results.

Table 8. Component and system β_D values for some common bridge types

Bridge Class	β_D							
	Longitudinal Direction			Transverse Direction				
	Piers	Bearings	Abutments	Bridge System	Piers	Bearings	Abutments	Bridge System
#232	0.88	0.73	0.67	0.73	0.86	0.71	0.59	0.71
#221	0.74	0.62	0.86	0.74	0.80	0.82	0.77	0.80
#121	0.76	0.59	0.79	0.76	0.81	0.64	0.69	0.81

4.3 Total Uncertainty for different bridge classes of a bridge stock

The fragility curve for the bridge system should be drawn for the β_{tot} value of the most critical component under the series connection assumption; the latter is typically the bearings in simply-supported bridges, and the piers in monolithic bridges (Nielson, 2005). As discussed in Stefanidou & Kappos (2017), the total uncertainty value is calculated at a component level according to equation 2, under the assumption of statistical independence, while the estimation of total uncertainty at system level is related to the structural system of the bridge; it is governed by pier (total) uncertainty for the case of monolithic bridge to deck connection, by bearings for simply supported bridges, and by abutments in single-span bridges.

$$\beta_{tot} = \sqrt{\beta_C^2 + \beta_D^2 + \beta_{LS}^2} \quad (2)$$

Details for the estimation of β_C and β_{LS} can be found elsewhere (Stefanidou & Kappos, 2017). Briefly, β_C values for bridge piers (based on analysis results) were found to vary from 0.31 to 0.41, according to the pier type, namely cylindrical, hollow cylindrical, rectangular, hollow rectangular and wall-type piers. Regarding β_{LS} for critical components, namely bridge piers, bearings and abutments, the values 0.35, 0.17 and 0.40 are proposed, respectively. Finally, as discussed in §4.2, a uniform (mean) β_D value for the longitudinal and transverse direction is recommended for the critical components of each bridge type. Comparing β_D values of bridge types 232, 221 and 121 (Table 8), it is obvious that the most critical issue for the uncertainty quantification is the structural system; monolithic bridges (types 221 and 121) have almost equal total uncertainty (0.64 and 0.62 respectively), while the uncertainty for simply supported varies, as expected, since different components are deemed critical in each structural system. Therefore, in order to estimate β_D for each component of the bridge types of a road network, based on the results of detailed analysis of the representative bridges of three frequent bridge types, differentiation according to the structural system is proposed (i.e. β_D values of bridge type 221 are used for monolithic pier-to-deck connection and values of bridge type 232 for the case of pier-to-deck connection through bearings).

Based on the above, the total uncertainty values (β_{tot}) for all bridge types in the stock are calculated according to equation 1 and summarised in Table 9. The total uncertainty for the bridge system (β_{tot}), calculated from bridge-specific fragility analysis, was found to vary from 0.72 to 0.82, values higher than 0.6 that is usually proposed in literature; it should be noted that these values also include uncertainty due to record-to-record variability.

Table 9. Component and system β_{tot} values for all bridge types of the inventory

Bridge type	Piers	Bearings	Abutments	β_{tot}
232	0.87	0.72	0.60	0.72
221	0.81	0.63	0.75	0.81
121	0.80	0.61	0.73	0.80
122	0.88	0.72	0.60	0.72
311	0.82	0.63	0.75	0.82
111	0.82	0.63	0.75	0.82
223	0.81	0.72	0.60	0.81
112	0.88	0.72	0.60	0.72
432	0.89	0.72	0.60	0.72
411	0.82	0.63	0.75	0.82
112	–	0.69	0.74	0.74
Single Span	0.87	0.72	0.60	0.72

5 BRIDGE-SPECIFIC VS. GENERIC FRAGILITY CURVES

Bridge-specific fragility curves for all bridges in the analysed stock are derived, following the methodology developed for bridge populations, to assess the relevance of bridge-specific fragility analysis. First, the effects of structural configuration (different pier, deck and pier-to-deck connection type), as well as of varying geometric properties, like pier height and bridge length, on bridge fragility are evaluated. Then, the differentiation of seismic fragility within

the same typological class is investigated, quantifying the range within which the damage thresholds vary for a given typological class and comparison of bridge-specific and generic, referring to the representative bridge of each class, fragility curves is performed, highlighting the importance of the bridge-specific approach in assessing a bridge stock.

5.1 Effect of structural configuration on bridge fragility

The methodology for bridge populations was applied to all bridges of the studied bridge stock, to derive structure-specific fragility curves. The effect of different pier, deck, pier-to-deck connection type and eventually the selected classification scheme on bridge fragility is depicted in Figures 13 to 17. The fact that these figures depict system fragility estimated under the assumption of series connection between components, should also be taken into account when interpreting the results.

Bridge fragility curves of the *generic* bridges of typological classes 111, 311, and 411, namely bridges with single-column cylindrical, multi-column cylindrical, and wall type piers, respectively, monolithically connected to the slab-type deck are depicted in Fig.13. The effect of different pier type on system fragility for the longitudinal and transverse direction of bridges having the same deck type and pier-to-deck connection is clear; bridges with single column piers are more vulnerable than bridges with multi-column cylindrical or wall-type piers. The most critical components in the case of monolithic pier-to-deck connection are bridge piers and abutments, therefore the relatively higher vulnerability in the transverse direction is due to the more unfavourable boundary conditions in this direction of the piers (close to cantilever action, hence higher bending moment). The use of multi-column bents results in lower seismic demand for each pier and, eventually, lower vulnerability, whereas wall-type piers have higher flexural and shear capacity (but higher seismic demand as well) compared to cylindrical single-column piers. Bridges with multi-column piers monolithically connected to the slab of the deck are less vulnerable in the longitudinal direction than bridges having the same deck and pier-to-deck connection type, but wall-type piers, whereas this is not the case for the transverse direction (strong axis of wall-type pier). Comparing the bridge-specific fragility curves of bridges with different pier types it is clear that the differences are important, mainly in the transverse direction and the lower limit states; seismic fragility of bridges with wall-type piers can be 60% (or more) lower than the relevant of bridges with single column piers. Therefore, the effect of pier type on seismic fragility is deemed important and the use of generic fragility curves is not appropriate; bridge-specific fragility curves are recommended instead.

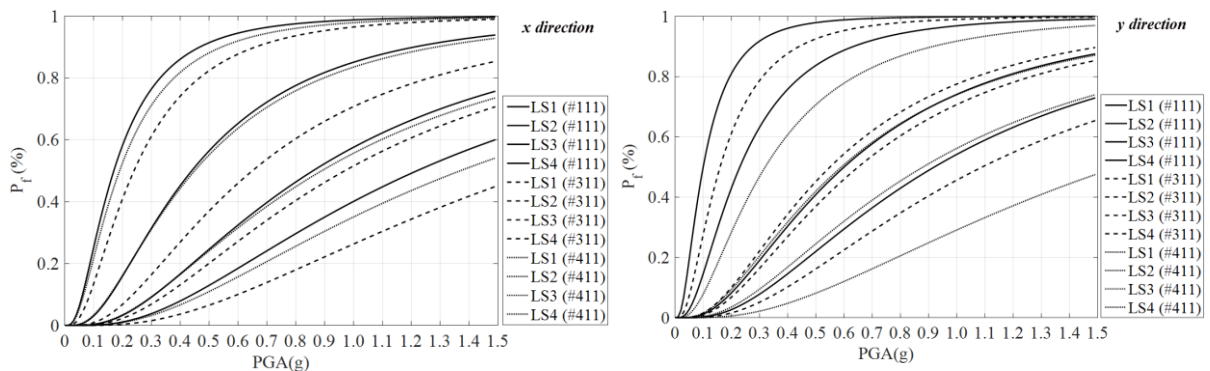


Fig. 13 – Fragility curves for the longitudinal (x) and transverse (y) direction of bridge classes 111, 311, and 411 (effect of pier type: single-column cylindrical, multi-column cylindrical, and wall type)

Comparing bridges with single-column cylindrical and hollow rectangular pier sections monolithically connected to the box-girder deck (classes 121 and 221, Fig. 14), the main finding is that bridges with hollow rectangular piers are less vulnerable, while the differences may become significant for the transverse direction and the higher limit states. Piers and abutments are the most critical components for the bridge classes considered herein. The differences are larger for LS1 and the longitudinal direction, since yielding of cylindrical piers occurs sooner, while the minor differences for the longitudinal direction and LS3 and LS4 are attributed to the critical component for the specific limit state (abutments); this is not the case if component fragilities are compared since the pier type is different. Differences in the transverse direction and LS3 and LS4 should be interpreted considering pier geometry and orientation of hollow rectangular pier in the transverse direction (strong axis). Based on the above remarks (and referring to Fig. 13), the effect of pier type on bridge fragility is considered important, mainly regarding the lower limit states, and should be duly accounted for.

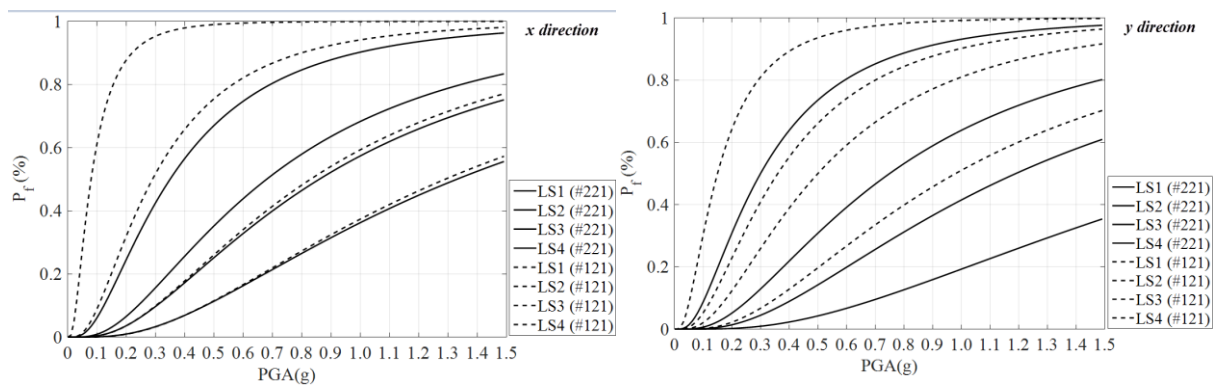


Fig. 14 – Fragility curves for the longitudinal and transverse direction of bridge classes 221 and 121 (effect of pier type: hollow rectangular vs. single-column cylindrical)

The differences in system fragility for the case of simply-supported bridges having hollow rectangular or wall-type piers connected through elastomeric bearings to the prestressed concrete beam deck (types 232 and 432, Fig. 15) are small, more so in the longitudinal direction; the main reason is that in this case bearings are the most critical component for most limit states. To this end, the use of generic fragility curves could, in principle, be acceptable for the case of simply-supported bridges with different pier types; namely for the case that wall type and hollow rectangular piers are used.

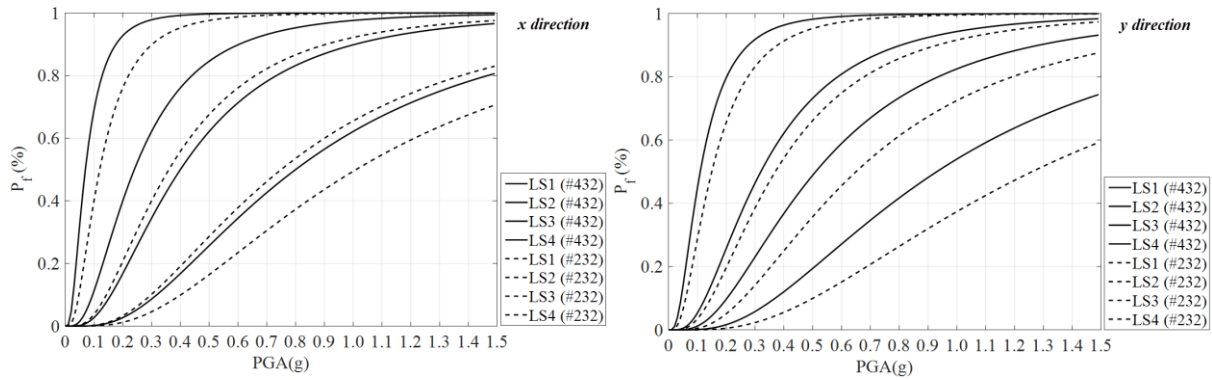


Fig. 15 – Fragility curves for the longitudinal and transverse direction of bridge classes 432 and 232 (effect of pier type: hollow rectangular vs. wall-type)

The effect of different deck type namely slab or box girder, on the fragility of bridges having single-column cylindrical piers connected to deck through elastomeric bearings (classes 122 and 112), is in general minor, as shown in Fig. 16. It should be noted, though, that the effect is larger for the longitudinal direction. The use of generic fragility curves for the case of simply-supported bridges with different deck type is, in general, acceptable, mainly for the transverse direction.

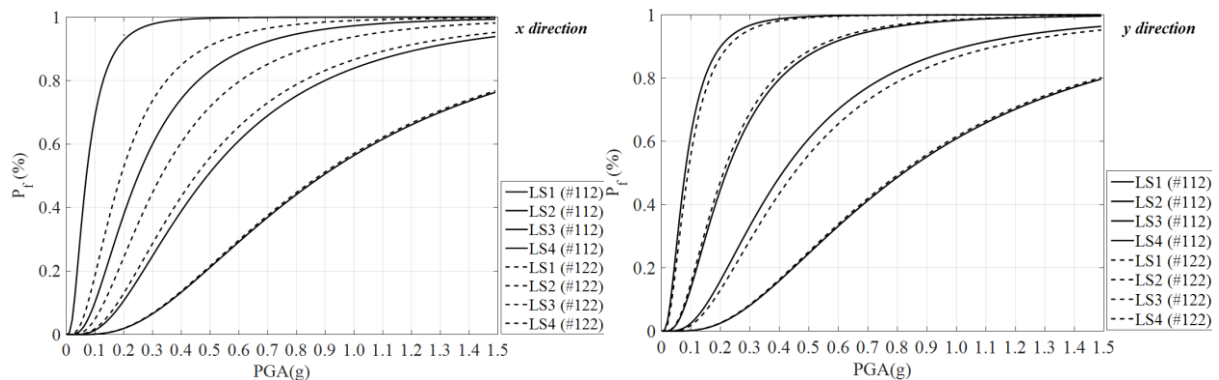


Fig. 16 – Fragility curves for the longitudinal and transverse direction of bridge classes type 112, type 122 (effect of deck type: slab or box girder)

Finally, the effect of pier-to-deck connection (monolithic or through elastomeric bearings) on bridges having single-column cylindrical piers and slab-type deck, is depicted in Fig. 17 (types 112 and 111). It is seen that fragility of monolithic bridges is lower for all limit states and in both directions. The latter is due to the fact that different components, namely bearings and piers, are critical for the seismic performance of each bridge class, mainly in the longitudinal direction.

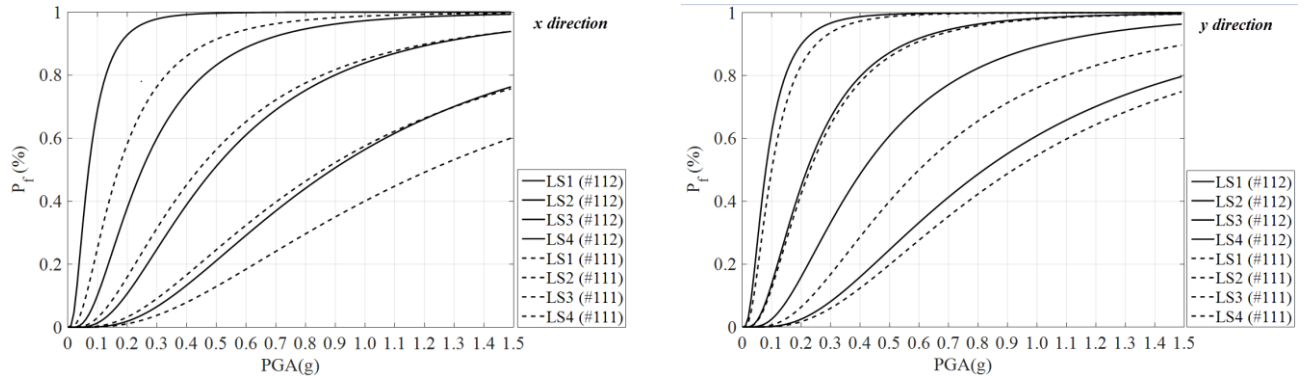


Fig. 17 – Fragility curves for the longitudinal and transverse direction of bridge classes 112 and 111 (effect of pier-to-deck connection: monolithic vs. through bearings).

From the comparison of bridge-specific fragility curves derived for the generic bridge in each typological class, it is concluded that bridge fragility varies among different classes, which establishes the importance of the classification scheme adopted. Among the features considered in defining the typological classes, the pier type and pier-to-deck connection type were found to affect bridge fragility the most, compared to the deck type (which is the most critical bridge component when non-seismic loads are considered). The maximum differentiation in fragility curves of different bridge classes was found in the case of monolithic pier-to-deck connection and varying pier types, because in that case piers are the most vulnerable component and their type (single-column cylindrical, multi-column cylindrical, hollow rectangular, wall, etc.) strongly affects the dynamic characteristics of the bridge and, hence, its seismic performance.

5.2 Effect of geometric properties on bridge fragility

The effect of pier height(s) and total bridge length on bridge fragility is evaluated comparing the bridge-specific limit state thresholds (mean PGA values) for *all* bridges and *each* bridge class of the inventory (Figures 20 to 22). The variation of threshold values is clear, highlighting the effect of bridge geometry (pier height and total length) on seismic fragility and the importance of bridge-specific fragility curves in the seismic assessment of a bridge stock. In Fig. 20, the variation of limit state threshold values in PGA terms with varying maximum pier height is presented. Since the range of pier heights and the number of piers are not accounted for, an equivalent height (H_{equiv}) is proposed (Eq. (3) and Fig. 21), considering the heights of all piers (h_i) and the number of piers (n), in order to evaluate the effect of pier height on system fragility; clearly this is a simplified way to address the issue, not appropriate for extreme cases, such as the presence of a short pier in the middle of the bridge (found in some poorly designed existing bridges).

$$n \cdot \frac{1}{h_{eq}^3} = \sum_i^n \frac{1}{h_i^3} \quad (3)$$

As seen in Fig. 21, bridges having shorter piers (lower h_{eq}) are in general more vulnerable, however it should be highlighted that the threshold values refer to the bridge system rather than the individual components. The general trend and the relevant limit state threshold variation is depicted in Fig. 21 for different bridge classes and limit states (piers are the most critical components for the cases shown).

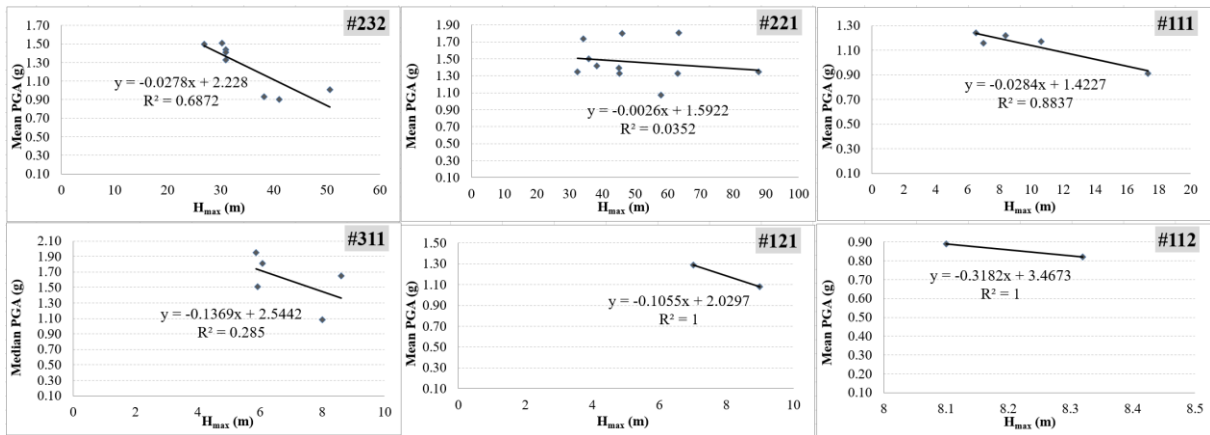


Fig. 20 – Effect of maximum pier height on seismic fragility of different bridge classes (mean PGA values for LS4)

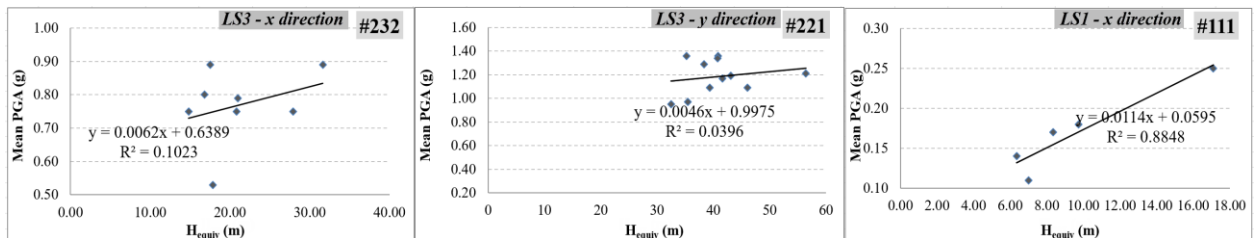


Fig. 21– Effect of equivalent pier height on seismic fragility of different bridge classes

Finally, based on Fig. 22, it appears that the effect of total length on bridge system fragility varies, depending on the bridge class and structural system; no clear trends can be identified in this case, as several other factors affect the calculated PGA thresholds.

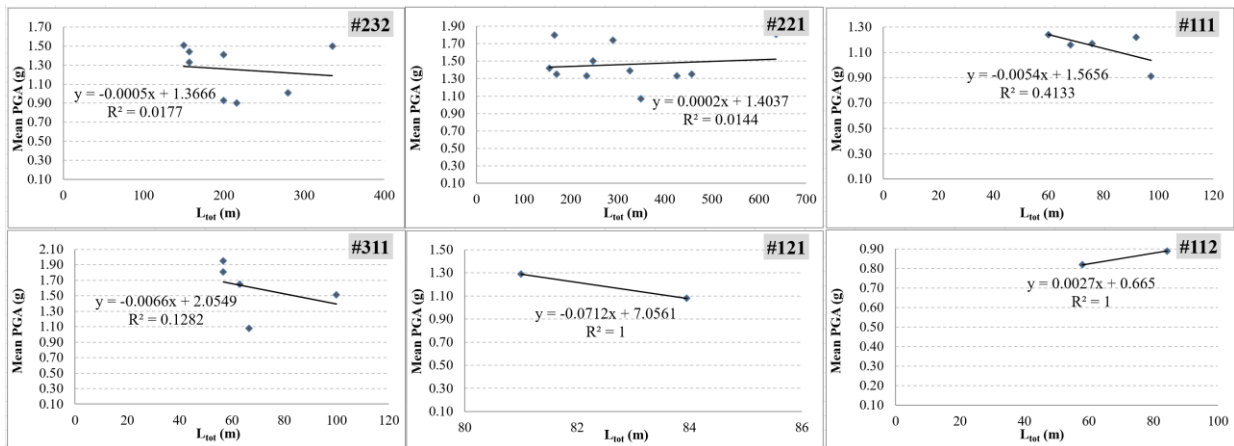


Fig. 22 – Effect of total bridge length on seismic fragility of different bridge classes

Summarising, the effect of geometric properties on bridge fragility is found to be significant, as the limit state thresholds for bridges classified within the same class may differ by up to 60%; hence, the necessity for bridge-specific fragility analysis clearly emerges.

5.3 Differentiation of seismic fragility within the same typological class

As already mentioned, most of the available methodologies in the literature propose the use of generic fragility curves for all bridges that fall within the same category, under the

assumption that the seismic performance of all bridges in the category is similar. The limitations of this assumption are investigated here, by considering the bridge-specific fragility curves for all bridges within the two most common classes of the studied road network (types 232 and 221, Fig. 12).

Table 10. Limit state thresholds in PGA terms for all bridges of typological class 232 (both directions)

232	Fragility (Direction x)				Fragility (Direction y)				L _{span} (m)	H _{pier} (m)	L _{tot} (m)	H _{max} (m)
	LS1	LS2	LS3	LS4	LS1	LS2	LS3	LS4				
1 (repr.)	0.12	0.36	0.75	1.01	0.15	0.37	0.65	1.26	40	21.0÷50.60	280	50.6
2	0.13	0.37	0.75	1.50	0.13	0.38	0.74	1.68	36.3÷37.50	9.4÷26.92	335.1	26.92
3	0.11	0.28	0.53	0.90	0.11	0.23	0.65	1.45	36	11.4÷41.01	216	41.01
4	0.12	0.32	0.80	0.93	0.16	0.32	0.70	0.94	40	12.94÷38.24	200	38.24
5	0.14	0.28	0.79	1.51	0.20	0.45	0.95	1.61	36.95÷38.05	16.3÷30.27	150	30.27
6	0.15	0.40	0.89	1.44	0.22	0.45	0.89	1.78	39.1÷39.50	12.75÷30.98	157.2	30.98
7	0.15	0.45	0.89	1.41	0.18	0.38	0.75	1.45	40	12.75÷30.98	200	30.98
8	0.13	0.30	0.75	1.33	0.12	0.28	0.55	1.49	39.1÷39.50	12.75÷30.98	157.2	30.98
mean	0.13	0.35	0.77	1.25	0.16	0.36	0.74	1.46			211.94	35.00
standard deviation	0.015	0.061	0.113	0.262	0.039	0.077	0.131	0.263			65.39	7.80
COV	11.11%	17.67%	14.66%	20.90%	24.61%	21.65%	17.84%	18.06%			30.85%	22.29%

Table 11. Limit state thresholds in PGA terms for all bridges of typological class 221 (both directions)

221	Fragility (Direction x)				Fragility (Direction y)				L _{span} (m)	H _{pier} (m)	L _{tot} (m)	H _{max} (m)
	LS1	LS2	LS3	LS4	LS1	LS2	LS3	LS4				
1 (repr.)	0.35	0.68	0.86	1.33	0.30	0.75	1.19	2.02	61.5÷112.1	41.30÷45.23	234.1	45.23
2	0.30	0.76	0.83	1.07	0.48	0.70	1.21	2.38	94.5÷160	55.00÷58.00	349	58
3	0.36	0.93	1.23	1.74	0.54	0.77	1.36	2.58	80÷120	34.20÷36.41	290	36.41
4	0.16	0.59	0.98	1.81	0.24	0.55	0.97	1.39	75.6÷120	28.12÷63.39	636.2	63.39
5	0.33	0.79	1.12	1.33	0.41	0.77	1.36	2.58	60.75÷101.5	34÷63.03	426	63.03
6	0.24	0.89	1.13	1.39	0.45	0.70	1.17	2.40	91÷144	39÷45.10	326	45.10
7	0.36	0.72	0.95	1.35	0.35	0.77	1.34	2.32	61÷107	29.12÷87.83	457	87.83
8	0.37	0.76	0.96	1.50	0.30	0.62	1.09	2.30	64.3÷118.6	35.86÷44.89	247.2	44.89
9	0.36	0.72	0.95	1.35	0.47	0.72	0.95	2.50	85	32.47	170	32.47
10	0.29	0.75	1.04	1.80	0.43	0.62	1.09	2.32	80÷86	46.08	166	46.08
11	0.41	0.65	0.82	1.42	0.42	0.75	1.29	2.05	75÷80	38.37	155	38.37
mean	0.32	0.75	0.99	1.46	0.40	0.70	1.18	2.26			314.23	50.98
standard deviation	0.070	0.098	0.131	0.231	0.091	0.074	0.147	0.341			147.49	15.97
COV	21.97%	13.09%	13.28%	15.81%	22.81%	10.60%	12.44%	15.11%			46.94%	31.32%

Table 12. Differentiation (%) in fragility of type 232 bridges compared to the representative bridge of the class.

Bridge	LS thresholds (Direction x)				LS thresholds (Direction y)			
	LS1	LS2	LS3	LS4	LS1	LS2	LS3	LS4
1	<i>Representative bridge of class 232</i>				<i>Representative bridge of class 232</i>			
2	-8	-3	0	-49	13	-3	-14	-33
3	8	22	29	11	27	38	0	-15
4	0	11	-7	8	-7	14	-8	25
5	-17	22	-5	-50	-33	-22	-46	-28
6	-25	-11	-19	-43	-47	-22	-37	-41
7	-25	-25	-19	-40	-20	-3	-15	-15
8	-8	17	0	-32	20	24	15	-18

Limit state thresholds for all bridges of classes 232 and 221 (namely bridges with hollow rectangular piers connected through bearings to prestressed beam deck and monolithically connected to box-girder bridge deck, respectively) are presented in Tables 10 and 11 in PGA terms. Mean, standard deviation and coefficient of variation (COV) values based on statistical analysis of results are presented and differentiation (percentage) of the bridge-specific limit state threshold compared to the relevant value of the representative bridge, is additionally provided (Tables 12 and 13) for each limit state and both longitudinal and transverse direction. The total bridge and span length, as well as the range of pier heights and maximum pier height, are also provided (Tables 10 & 11) to highlight the effect of different geometric properties of fragility curves of bridges classified within the same class.

Table 13. Differentiation (%) in fragility of type 221 bridges compared to the representative bridge of the class.

Bridge	LS thresholds (Direction x)				LS thresholds (Direction y)			
	LS1	LS2	LS3	LS4	LS1	LS2	LS3	LS4
1	<i>Representative bridge of class 221</i>				<i>Representative bridge of class 221</i>			
2	14	-12	3	20	-60	7	-2	-18
3	-3	-37	-43	-31	-80	-3	-14	-28
4	54	13	-14	-36	20	27	18	31
5	6	-16	-30	0	-37	-3	-14	-28
6	31	-31	-31	-5	-50	7	2	-19
7	-3	-6	-10	-2	-17	-3	-13	-15
8	-6	-12	-12	-13	0	17	8	-14
9	-3	-6	-10	-2	-57	4	20	-24
10	17	-10	-21	-35	-43	17	8	-15
11	-17	4	5	-7	-40	0	-8	-1

It is seen that the differentiation of limit state thresholds among bridges of the same category is typically up to 35%; however, for the case of bridges with hollow rectangular piers connected through bearings to the prestressed concrete beam deck (type 232) the underestimation may reach 50% and for bridges with hollow rectangular piers monolithically connected to the box-girder deck, the underestimation may reach 80% (Tables 12 and 13). The differences are, in general, larger in the case of monolithic bridges and the transverse direction. Furthermore, it

should be outlined that differentiation in limit state thresholds (mean value), compared to that of the representative bridge of the class, is lower when the geometric properties (pier height, bridge length, etc.) are similar.

5.3.1. Comparison of bridge-specific and generic fragility curves

Bridge-specific fragility curves for all bridges in class 232 (hollow rectangular piers connected through bearings to the prestressed concrete beam deck) and 221 (piers monolithically connected to the box-girder bridge deck) were derived and compared to the fragility curves of the generic bridge, representative of each class. The results are depicted in Figures 23 and 24, along with upper and lower threshold values (dashed lines - range of thresholds) for each limit state.

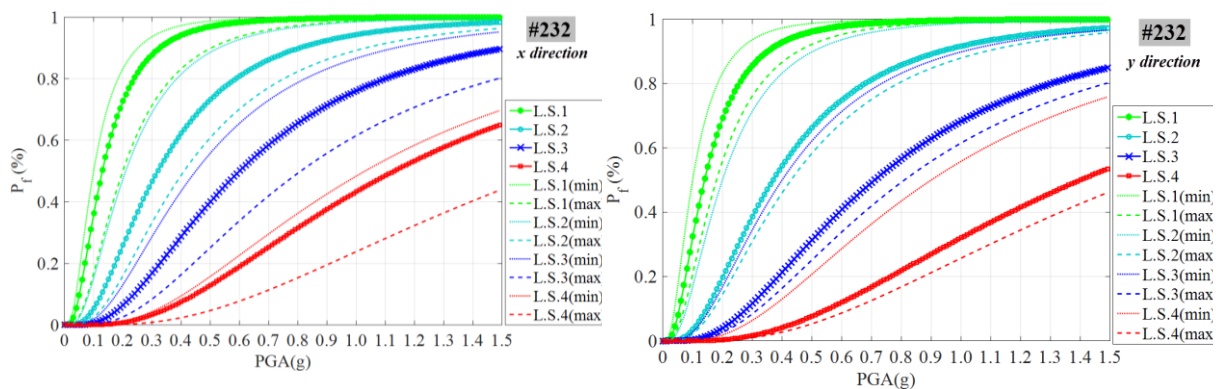


Fig. 23 – Fragility of the generic bridge in class type 232 and range of damage thresholds

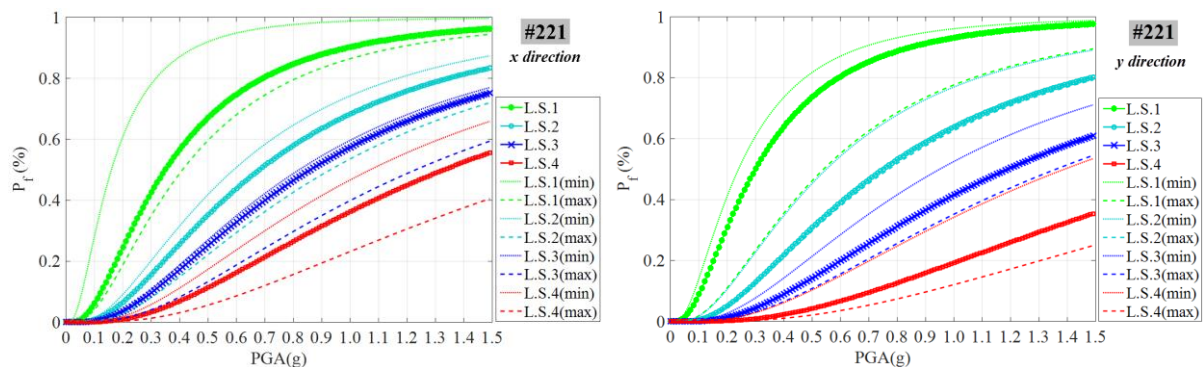


Fig. 24 – Fragility of the generic bridge in class type 221 and range of damage thresholds

As far as bridge class 232 is concerned, the variation of upper and lower level fragilities compared to that of the generic bridge is small, therefore fragility curves of the bridge selected as representative can be used for all bridges that fall within the same category for the longitudinal direction and LS1 to LS3. The range of threshold values is fairly narrow in the longitudinal direction (25% variation from the generic bridge) for lower limit states, however it broadens for higher earthquake intensity and limit states and for the transverse direction, being dependent both on the component that is critical for each limit state and the direction. The variation of upper and lower level fragilities for bridge class type 221 is smaller for LS2 to LS4 but larger for LS1. In general, the use of the fragility curves of the generic bridge for

all those in the same category may underestimate or overestimate fragility by up to 35%, however in some cases (i.e. LS1 for bridge class 221 and LS4 for class 221) the underestimation is up to 50%.

6 CONCLUSIONS

The relevance of bridge-specific fragility analysis was assessed herein. First, the effect of varying component and system properties on both capacity and (seismic) demand was quantified. Then the effect of structural system and key geometric properties on bridge fragility was assessed. The foregoing allowed to subsequently check the limitations of the assumption that generic fragility curves can be used for bridges classified within the same category, referring to a realistic bridge stock. Both structural system (pier type, deck type and pier-to-deck connection) and geometric properties were found to substantially affect bridge fragility. The use of generic fragility curves may become acceptable under certain circumstances, namely for bridges with the same pier type and pier-to-deck connection having a different deck type, and bridges with the same deck type and pier-to-deck connection when pier type is either wall-type or hollow rectangular (i.e. very stiff cross section). However, this is only true when bridge geometries, namely pier heights and bridge length, are similar, since the effect of geometric properties on bridge fragility was found to be significant (up to 60%). Moreover, the use of generic fragility curves for bridges belonging to the same class were found to overestimate (up to 35%) or underestimate (up to 50%) bridge fragility, depending on the limit state and critical direction considered. The use of generic fragility curves seems more consistent for simply-supported bridges and the limit states 2 and 3.

Summarising, the most important findings are listed below:

- Limit state thresholds (bridge capacity) are highly affected by component properties and the demand parameter selected as a proxy for damage; hence, use of component-specific values is relevant and often necessary.
- Uncertainty in seismic demand generally increases with earthquake intensity, being affected by the inelastic behaviour of the component studied, the record-to-record variability, and the criteria for earthquake motion selection; uncertainty level varies among critical components (piers-abutments-bearings) and bridge directions.
- The total uncertainty of bridge system (β_{tot}), calculated in bridge-specific fragility analysis, was found to vary from 0.72 to 0.82, which are higher than 0.6, the value commonly used in the literature; it should be noted that these values also include uncertainty due to record-to-record variability.
- Pier type has an important effect on system fragility for the case of bridges with box-girder decks and monolithic pier-to-deck connection, as piers are the most critical component for this bridge type. The effect of pier type on the fragility of simply-supported (through elastomeric bearings) bridges is lower, as the bearings are the most critical component for this bridge class for most limit states.
- Bridges with single-column cylindrical piers monolithically connected to slab or box-girder decks are more vulnerable than similar bridges having multi-column cylindrical, wall-type, or hollow rectangular piers. Among bridges with monolithic pier-to-deck connection, those

with hollow rectangular piers monolithically connected to box-girder deck are the less vulnerable class (transverse direction).

- The effect of deck type on fragility of bridges having single-column cylindrical piers connected to the deck through elastomeric bearings is in general minor.
- Regarding the effect of pier-to-deck connection, monolithic bridges are less vulnerable for all limit states and both bridge directions compared to simply-supported bridges; different components are critical in each case (piers and bearings, respectively).
- The variation of limit state thresholds within a bridges class, due to different pier heights and total length, highlights the need for bridge-specific fragility curve development, as limit state thresholds for bridges with varying geometric properties (belonging to the same class) may vary by up to 60%.
- The use of generic bridge fragility curves for all bridges in a typological class may underestimate or overestimate fragility, typically by up to 35%; however in some cases the underestimation may reach 50% (or even more), which is clearly an issue of concern and a good reason for using bridge-specific curves.
- For simply-supported bridges (prestressed concrete beam deck, bearing-supported to the piers), the range of LS threshold values is generally fairly narrow for the longitudinal direction and the lower limit states (LS2 & LS3), but it increases for higher earthquake intensity and higher limit states (heavy damage, failure). For the transverse direction, the variation is higher for the lower limit states as well.
- For the studied case of monolithic bridges (hollow rectangular piers monolithically connected to the box-girder of the deck), the range of limit state thresholds is broader, mainly for the lower limit states and the transverse direction, as the seismic performance of monolithic bridges is highly dependent on varying properties and boundary conditions of the piers, which strongly affect the dynamic characteristics of the bridge. However, the range is narrower for higher limit states (LS3 & LS4), compared to simply-supported bridges.

Based on the above, the need for bridge-specific fragility analysis emerges since, the use of generic fragility curves can, in several cases, significantly affect the reliability of a road network assessment. Therefore, the concept of bridge-specific fragility analysis, recently proposed in literature, seems to be a step in the right direction.

ACKNOWLEDGEMENTS

This research has been co-financed by the European Union (European Social Fund – ESF) and Greek national funds through the Operational Programme “Education and Lifelong Learning” of the National Strategic Reference Framework (NSRF) – Research Funding Program: *ARISTEIA II: Reinforcement of the interdisciplinary and/or interinstitutional research and innovation*. The authors would like to thank Egnatia Odos S.A. for providing the data for the case study bridges, and all participants to the RETIS-Risk research programme for their cooperation in this multi-disciplinary project.

7 REFERENCES

- Avşar, Ö., Yakut, A., & Caner, A. (2011). Analytical Fragility Curves for Ordinary Highway Bridges in Turkey. *Earthquake Spectra*, 27(4), 971–996.
- Banerjee, S., & Shinozuka, M. (2007). Nonlinear Static Procedure for Seismic Vulnerability Assessment of Bridges. *Computer-Aided Civil and Infrastructure Engineering*, 22(4), 293–305.
- Basoz, N., Kiremidjian, A., King, S., & Law, K. (1999). Statistical Analysis of Bridge Damage Data from the 1994 Northridge, CA, Earthquake. *Earthquake Spectra*, 15(1), 25–54.
- Berry, M., & Eberhard, M. (2003). *Performance Models for Flexural Damage in Reinforced Concrete Columns*. University of Washington.
- Biskinis, D. E., & Fardis, M. N. (2010). Deformations at flexural yielding of members with continuous or lap-spliced bars. *Structural Concrete*, 11(2), 127–138.
- Biskinis, D., & Fardis, M. N. (2010). Flexure-controlled ultimate deformations of members with continuous or lap-spliced bars. *Structural Concrete*, 11, 93–108.
- Boussias, E., Palios, X., Alexakis, C., Strepelias, E., Fardis, M., & Raptopoulos, S. (2008). Experimental and analytical study of seismically isolated bridges with or without additional damping. In *3rd Hellenic Conference of Earthquake Engineering and Engineering Seismology*. 5-7 November, Athens, Greece (in Greek).
- Caltrans Structures Seismic Design Criteria. (2010). Sacramento, California.
- Cardone, D. (2013). Displacement limits and performance displacement profiles in support of direct displacement-based seismic assessment of bridges. *Earthquake Engineering & Structural Dynamics*, 43(8), 1239–1263.
- Cardone, D., Perrone, G., & Sofia, S. (2011). A performance-based adaptive methodology for the seismic evaluation of multi-span simply supported deck bridges. *Bulletin of Earthquake Engineering*, 9(5), 1463–1498.
- Cardone, D., Perrone, G., & Dolce, M. (2007). Seismic risk assessment of highway bridges. In *1st US-Italy Seismic Bridge Workshop*. Pavia, Italy.
- Choi, E. (2004). Seismic fragility of typical bridges in moderate seismic zones. *Engineering Structures*, 26(2), 187–199.
- Choi, E., DesRoches, R., & Nielson, B. (2004). Seismic fragility of typical bridges in moderate seismic zones. *Engineering Structures*, 26(2), 187–199.
- Crowley, H., Colombi, M., Silva, V., Monteiro, R., Ozcebe, S., Fardis, M., ... Askouni, P. (2011). *SYNER-G: Systemic Seismic Vulnerability and Risk Analysis for Buildings, Lifeline Networks and Infrastructures Safety Gain*. University of Pavia, Italy.
- De Felice, G., & Giannini, R. (2010). An Efficient Approach for Seismic Fragility Assessment with Application to Old Reinforced Concrete Bridges. *Journal of Earthquake Engineering*, 14(2), 231–251.
- DesRoches, R., Padgett, J., Ramanathan, K., & Dukes, J. (2012). *Feasibility Studies for Improving Caltrans Bridge Fragility Relationships*. Rep. CA12-1775, Georgia Institute of Technology, Atlanta, U.S.A.
- Dukes, J. D. (2013). *Application of Bridge Specific Fragility Analysis in the Seismic Design Process of Bridges in California*. PhD Thesis, Georgia Institute of Technology, Georgia.
- Dutta, A. (1999). *On Energy Based Seismic Analysis and Design of Highway Bridges*. State University of New York, Buffalo.
- Dutta, A., & Mander, J. B. (1998). Seismic fragility analysis of highway bridges. In *INCEDE-MCEER Center-to-Center Workshop on Earthquake Engineering Frontiers in Transportation Systems*. Tokyo, Japan.
- Elnashai, A. S., Borzi, B., & Vlachos, S. (2004). Deformation-based vulnerability functions for

- RC bridges. *Structural Engineering and Mechanics*, 17(2), 215–244.
- Erduran, E., & Yakut, A. (2004). Drift based damage functions for reinforced concrete columns. *Computers & Structures*, 82, 121–130.
- FHWA. (2006). *Seismic Retrofitting Manual for Highway Structures: Part I-Bridges*. FHWA-HRT-06-032.
- Ghosh, J., Padgett, J. E., & Dueñas-Osorio, L. (2013). Surrogate modeling and failure surface visualization for efficient seismic vulnerability assessment of highway bridges. *Probabilistic Engineering Mechanics*, 34, 189–199.
- HAZUS: *Earthquake loss estimation methodology*, 2015. Technical Manual, National Institute of Building for the Federal Emergency Management Agency, Washington, D.C.
- Hwang, H., Liu, J. B., & Chiu, Y.-H. (2001). *Seismic Fragility Analysis of Highway Bridges*. The University of Memphis.
- Kappos, A. J. (1991). Analytical Prediction of the Collapse earthquake for R/C buildings : Suggested Methodology. *Earthquake Engineering & Structural Dynamics*, 20, 167–176.
- Karim, K. R., & Yamazaki, F. (2001). Effect of earthquake ground motions on fragility curves of highway bridge piers based on numerical simulation. *Earthquake Engineering & Structural Dynamics*, 30(12), 1839–1856.
- Karim, K. R., & Yamazaki, F. (2003). A simplified method of constructing fragility curves for highway bridges. *Earthquake Engineering & Structural Dynamics*, 32(10), 1603–1626.
- Konstantinidis, D., Kelly, J. M., & Makris, N. (2008). *Experimental investigations on the seismic response of bridge bearing*. Berkeley.
- Lee, J.-H., Choi, J.-H., Hwang, D.-K., & Kwahk, I.-J. (2014). Seismic performance of circular hollow RC Bridge columns. *KSCE Journal of Civil Engineering*, 1–12.
- Lu, Y., Gu, X., & Guan, J. (2005). Probabilistic Drift Limits and Performance Evaluation of Reinforced Concrete Columns. *Journal of Structural Engineering, ASCE*, 131(6), 966–978.
- Mackie, K. R., & Stojadinović, B. (2007). R-Factor Parameterized Bridge Damage Fragility Curves. *Journal of Bridge Engineering*, 12(4), 500–510.
- Mackie, K., & Stojadinović, B. (2004). Fragility Curves For Reinforced Concrete Highway Overpass Bridges. In *13th World Conference on Earthquake Engineering*. Vancouver, B.C., Canada.
- Mander, J. B., Priestley, M. J. N., & Park, R. (1988). Theoretical Stress-Strain Model for Confined Concrete. *Journal Of Structural Engineering*, 114(8), 1804–1826.
- Mander, J., & Basöz, N. (1999). *Enhancement of the Highway Transportation Lifeline Module in HAZUS*. Final Pre-Publication Draft (type 7) prepared for National Institute of Building Sciences (NIBS).
- McKeena, F., & Fenves, G. L. (2015). Open System for Earthquake Engineering Simulation. Pacific Earthquake Engineering Research Center.
- Moschonas, I. F., Kappos, A. J., Panetsos, P., Papadopoulos, V., Makarios, T., & Thanopoulos, P. (2009). Seismic fragility curves for greek bridges: methodology and case studies. *Bulletin of Earthquake Engineering*, 7(2), 439–468.
- Nielson, B. G. (2005). *Analytical Fragility Curves for Highway Bridges in Moderate Seismic Zones Analytical Fragility Curves for Highway Bridges in Moderate Seismic Zones*. PhD Thesis, Georgia Institute of Technology, Atlanta.
- Nielson, B. G., & DesRoches, R. (2007a). Analytical Seismic Fragility Curves for Typical Bridges in the Central and Southeastern United States. *Earthquake Spectra*, 23(3), 615.
- Nielson, B. G., & DesRoches, R. (2007b). Seismic fragility methodology for highway bridges using a component level approach. *Earthquake Engineering and Structural Dynamics*, 36, 823–839.
- Papanikolaou, V. K. (2012). Analysis of arbitrary composite sections in biaxial bending and

- axial load. *Computers and Structures*, 98-99, 33–54.
- Priestley, M. J. N., & Ranzo, G. (2000). Seismic performance of large rc circular hollow columns. In *12th World Conference of Earthquake Engineering* (pp. 1–8). Auckland, New Zealand.
- Priestley, M. J. N., Seible, F., & Calvi, G. M. (1996). *Seismic Design and Retrofit of Bridges*. In J. Willey . New York.
- Ramanathan, K. N. (2012). *Next Generation Seismic Fragility Curves for California Bridges Incorporating the Evolution in Seismic Design Philosophy*. PhD Thesis, Georgia Institute of Technology, Georgia.
- Shinozuka, M., Feng, M. Q., Kim, H., & Kim, S.-H. (2000). Nonlinear Static Procedure for Fragility Curve Development. *Journal of Engineering Mechanics, ASCE*, 126(12), 1287–1295.
- Shinozuka, M., Feng, M. Q., Lee, J., & Naganuma, T. (2000). Statistical Analysis of fragility curves. *Journal of Engineering Mechanics, ASCE*, 126(12), 1224–1231.
- Stefanidou, S. P. (2017). Software for Bridge-Specific Fragility Analysis. *MOJ Civil Engineering*, 3(5), 1–7.
- Stefanidou, S.P. & Kappos, A. J. (2015). Methodology for the development of structure-specific fragility curves for bridges in a roadway network. Proceed. COMPDYN 2015, Crete, vol. I, 1780-1798.
- Stefanidou, S. P. & Kappos, A. J. (2017). Methodology for the development of bridge-specific fragility curves. *Earthquake Engineering & Structural Dynamics*, 46, 73–93.
- Tavares, D. H., Padgett, J. E., & Paultre, P. (2012). Fragility curves of typical as-built highway bridges in eastern Canada. *Engineering Structures*, 40, 107–118.
- Tsionis, G., & Fardis, M. N. (2012). Seismic Fragility of Concrete Bridges with Deck Monolithically Connected to the Piers or Supported on Elastomeric Bearings. In *15th World Conference of Earthquake Engineering*. Lisbon, Portugal.
- Yi, J., Kim, S., & Koshiyama, S. (2007). PDF interpolation technique for seismic fragility analysis of bridges. *Engineering Structures*, 29(7), 1312–1322.
- Zhang, J., Huo, Y., Brandenburg, S. J., & Kashighandi, P. (2008). Effects of structural characterizations on fragility functions of bridges subject to seismic shaking and lateral spreading. *Earthquake Engineering and Engineering Vibration*, 7(4), 369–382.
- Zhong, J., Gardoni, P., & Rosowsky, D. (2012). Closed-form seismic fragility estimates, sensitivity analysis and importance measures for reinforced concrete columns in two-column bents. *Structure and Infrastructure Engineering*, 8(7), 669–685.

ANNEX A – β values for all pier types (*global demand parameter, see table 4*)

Hollow Cylindrical Piers							
	β_0	β_1	β_2	β_3	β_4	β_5	R^2
δ_1/H	-5.996	-0.445	-0.007	-0.198	-0.470	-0.117	0.74
δ_2/H	-5.285	-0.385	+0.224	-0.352	+0.106	-0.0013	0.82
δ_3/H	-3.867	-0.287	-0.084	-0.486	-0.433	+0.375	0.82
δ_4/H	-5.863	-0.308	-0.119	-0.885	-0.219	+0.031	0.80
Rectangular Piers (Strong direction h)							
	β_0	β_1	β_2	β_3	β_4	β_5	R^2
δ_1/H	-5.695	-0.595	+0.014	-0.076	-0.549	+0.080	0.61

δ_2/H	-5.520	-0.736	+1.315	-0.200	-0.120	+0.018	0.85
δ_3/H	-0.643	-0.673	+1.165	-0.210	-0.262	+0.975	0.62
δ_4/H	-2.861	-0.611	+0.426	-0.146	-0.114	+0.249	0.79
Rectangular Piers (Weak direction b)							R^2
	β_0	β_1	β_2	β_3	β_4	β_5	
δ_1/H	-5.290	-0.386	+1.350	-0.106	-0.526	+0.101	0.74
δ_2/H	-5.350	-0.718	+1.073	-0.085	-0.089	+0.021	0.75
δ_3/H	-1.531	-0.639	+0.867	-0.284	-0.109	+0.772	0.67
δ_4/H	-2.518	-0.630	+0.845	-0.252	-0.106	+0.386	0.60
Hollow Rectangular Piers (Strong direction h)							R^2
	β_0	β_1	β_2	β_3	β_4	β_5	
δ_1/H	-7.606	+0.912	+0.957	-0.175	-0.203	-0.502	0.63
δ_2/H	-5.952	+0.809	+0.857	-0.076	-0.020	-0.133	0.60
δ_3/H	-4.483	+0.774	+0.459	+0.313	-0.094	-0.028	0.66
δ_4/H	-4.415	+0.796	+0.264	-0.091	-0.004	-0.083	0.68
Hollow Rectangular Piers (Weak direction b)							R^2
	β_0	β_1	β_2	β_3	β_4	β_5	
δ_1/H	-5.715	+0.714	-0.629	-0.104	-0.181	-0.359	0.87
δ_2/H	-5.422	+0.751	-0.364	-0.020	-0.075	-0.008	0.90
δ_3/H	-3.401	+0.728	-0.648	-0.156	-0.314	+0.071	0.97
δ_4/H	-1.732	+0.721	-0.285	-0.573	-0.413	-0.250	0.87
Wall Piers (Strong direction h)							R^2
	β_0	β_1	β_2	β_3	β_4	β_5	
δ_1/H	-6.650	-0.447	-0.230	-0.142	-0.423	+0.067	0.86
δ_2/H	-4.021	-0.804	-0.645	+0.390	-0.102	-0.018	0.94
δ_3/H	+2.580	-0.793	-1.003	+0.482	-0.306	+1.096	0.64
δ_4/H	-3.450	-0.842	-0.054	+0.190	+0.069	+0.082	0.70
Wall Piers (Weak direction b)							R^2
	β_0	β_1	β_2	β_3	β_4	β_5	
δ_1/H	-5.957	-0.861	+0.707	-0.096	-0.690	+0.115	0.67
δ_2/H	-5.681	-0.871	+0.164	-0.062	-0.266	+0.044	0.88
δ_3/H	0.096	-0.810	-0.057	-0.086	-0.339	+1.075	0.70
δ_4/H	-3.91	-0.864	+0.085	+0.036	-0.079	+0.009	0.85